REMOTE SENSING IN THE REFLECTIVE SPECTRUM: A POWERFUL AND APPLIED TECHNOLOGY FOR TERRESTRIAL ECOSYSTEM SCIENCE

Arnon Karnieli

Address: Sede Boker Campus, 84990, Israel

Phone: +972-8-6596855

Fax: +972-8-6596858

E-mail: karnieli@bgu.ac.il

Affiliation and title: The Remote Sensing Laboratory, Jacob Blaustein Institutes for Desert Research, Ben-Gurion University of the Negev, Professor

ABSTRACT

Combining remote sensing techniques and methods with ecosystem science is challenging since the former has several notable benefits that offer a great number of advanced applications to terrestrial ecology in both spatial and temporal domains. Understanding the spectroscopy foundations and principles can open new horizons to ecologists by introducing a large variety of data, along with their algorithms and processing techniques, which are not be able to be achieved by traditional data collection methods. In this regard, the Chapter, which was compiled by a remote sensing specialist, reviews remote sensing capabilities for terrestrial ecology and provides the readers with detailed information on remote sensing means, algorithms, and techniques. The review contains four sections on: (1) past, current, and future spaceborne broadband and hyperspectral instruments and platforms; (2) spectral indices, including broad and narrow spectral indices for vegetation, soil, and other environmental substrates; (3) spectral analysis methods, including multivariable analysis, multitemporal data processing, phenology studies, and multi-source data fusion; and (4) a tabular summary of the key ecological variables with respect to their analysis methods, main spectral bands, and the preferred type of remote sensing platform. The summary notes several fundamental challenges in the path toward better integrating the two disciplines. The review is focused on the reflective part of the spectrum, i.e., the visible, near, and shortwave infrared regions; however, other regions, such as the thermal and microwave, are excluded. Moreover, the review mainly describes the spectral dimension of remote sensing, leaving the related image analysis techniques for another document.

Keywords: spaceborne platforms and instrumentation; spectral indices and algorithms; narrow bands; hyperspectral; spectral analysis; multivariable analysis; multitemporal analysis; phenological studies; ecological variables

1 INTRODUCTION

Remote sensing is the science and technology of deriving information about a target (material, object, or phenomenon) from measurements made at a distance and analyzing the interrelationships between the target and the reflected or emitted electromagnetic radiation. The electromagnetic spectrum comprises the full range of all radiation types from very short waves (e.g., gamma rays) to very long ones (e.g., radio and television), which characterize light. Although, in the wide sense, remote sensing can be used by a large number of disciplines with numerous applications (e.g., biomedical engineering, astrophysics, etc.) this Chapter focuses only on earth observation remote sensing. In this regard and despite the fact that the electromagnetic spectrum is continuous, the most applicative spectral regions for terrestrial ecosystem observations are the near ultraviolet (NUV, 0.3-0.4 μm), the visible (VIS, 0.4-0.7 μm), subdivided to blue (B, 0.4-0.5 μm), green (G, 0.5-0.6 μm), and red (R, 0.6-0.7 μm), the red-edge (RE, 0.7-0.8 μm), the near infrared (NIR, 0.8-1.1 μm), the shortwave infrared (SWIR, 1.1-4.5 μm), thermal infrared (TIR, 4.5-14 μm), and microwave (0.3-100 cm). These wavelength intervals, called spectral bands, were defined according to the physical property and the specific application of each region. Therefore, different technology and sensors are needed to acquire data from a particular region and in conjunction with a specific application.

The sun is the main source of radiation to *passive remote sensing sensors*; thus, *reflected radiation* refers to light that is returned from the detected target in the *reflective* spectral region (0.3-4.5 μm). However, since all materials at temperatures above absolute zero, 0°K, send out radiation, *emitted radiation* is connected to the thermal properties of the substance. In contrast to the passive sensors, *active sensors* both transmit pulses of energy to the target and record the backscattered pulses. Thus active systems, typically radars and lasers, control the length, timing, intensity, and polarization of the transmitted signal.

According the above definition of remote sensing, it can be implemented from any distance as long as there is no physical contact between the measuring device and the target. Consequently, remote sensing measurements can be carried out in the laboratory, in the field, from elevated platforms, and from airborne systems at different heights in the atmosphere, as well as from spaceborne systems in space. Historically, earth observations were filmed by cameras with spectral widths limited only to the *photographic region* (0.3-0.9 μm). In the last decades, the analog films were replaced by digital instruments that have notable advantages. First, they enlarged the applicative spectral region using a variety of detectors. Furthermore, the digital data can be stored, manipulated, transmitted, and archived by computers.

Remote sensing data are characterized by four types of resolutions that constitute the smallest observable (measurable) differences, namely, spatial, radiometric, spectral, and temporal resolutions. *Spatial resolution* refers to the finest angular (termed *instantaneous field of view*, IFOV) or linear separation (determined by the pixel size) between two objects that can be resolved by the sensor. *Radiometric resolution* is the number of digital levels that a sensor can use to express the variability of gray levels (brightness values) within the data. Radiometric resolution determines the information content of the image such that the more levels, the more details can be expressed. The radiometric resolution is determined by the number of bits within which the digital information is encoded and expressed in binary notation. For example, the acquisition level of an 8-bit system has (2^8 =) 256 gray levels confined within a dynamic range between 0 and 256. The *spectral resolution* characterizes the number and width of spectral bands used by the remote sensing system. The more numerous and narrower spectral bands enable the diagnostic absorption features to be observed, thus facilitating the identification of bio-physio-chemical processes in vegetation, soils, rock, and minerals (see Subsection 2.8 for more details). Finally, the *temporal resolution* is the revisit time of a specific sensor to acquire data from a specific location of earth. Revisit time can range from several minutes to several days, depending on the orbital characteristics of the satellite, the latitude of the target, the swath width of the sensor, and the pointing (tilting) capability of the system.

Remote sensing has several notable benefits that offer a great number of advanced applications in both spatial and temporal domains. First, remote sensing can be applied to spectral regions that are beyond the human sense of sight, thus enabling the discovery of extrasensory materials, objects, and phenomena. Measurements are unobtrusive and do not destroy the substrate, allowing periodic and repetitive sampling processes. From the spatial point of view, traditional data collection in the field is limited to the plot/local scales. On the other hand, spaceborne remote sensing covers regional to global views, even over inaccessible sites and under extreme conditions. Thus it enables observing the causes and effects of climate and environmental changes to be assessed. Spaceborne observations have a constant revisit time that allows repetitive geo-referenced looks at the same area. Modern remote sensing produces digital data, capable of being numerically manipulated within and among the spectral bands for enhancing the studied object. Consequently, understanding the spectroscopy foundations and principles can open new horizons to users by introducing a large variety of data, along with their algorithms and processing techniques, which are not be able to be achieved by traditional data collection methods.

Since the early development of digital remote sensing and spectroscopy technologies, they have played a crucial role in terrestrial ecosystem science, which has gradually increased throughout the years. This is primarily due to the ability of remote sensing to provide essential biophysical variables for ecological models, such as vegetation indices, leaf area index, land surface temperature, and many more, as described in Section 3. This source of valuable data appears in a large variety of spatial scales (plot, local, regional, national, continental, and global) and temporal scales (from minutes to days). In this regard, Plummer (2000) defined four approaches for linking remotely sensed data and ecological process models at a range of spatial and temporal scales: (1) using remotely sensed data to provide estimates of the variables required to drive ecological process models; (2) using remotely sensed data to test, validate, or verify the predictions of ecological process models; (3) using remotely sensed data to update or adjust ecological process model predictions; and (4) using ecological process models to understand remotely sensed data.

The Chapter is aimed at reviewing the abovementioned remote sensing capabilities that ensure advanced terrestrial ecosystem studies and applications. Note that the review is focused only on the *reflective spectrum*, this is to say, the part of the spectrum containing the visible, near and shortwave infrared regions, and therefore, the thermal and microwave instruments (e.g., radar, LIDAR) and their respective missions are excluded. Moreover, the review mainly describes the spectral dimension of remote sensing, leaving the related image analysis techniques for another document. Section 2 describes the most applied past, present, and future remote sensing instruments and platforms, distinguishing between the ones with different spatial and spectral resolutions. Section 3 reviews the most commonly used spectral indices that are applied to broad and narrow bands, for vegetation, soil, and other applications. Section 4 covers several spectral analysis methods, including multivariate spectral analysis, multitemporal data processing, and phenological studies. Key ecological variables are tabulated in Section 5 with respect to their analysis mean, their main spectral bands, and the preferred type of remote sensing platform. The Summary and Conclusions section lists several fundamental challenges on the way toward better integrating the remote sensing and terrestrial ecology disciplines.

2 INSTRUMENTATION AND PLATFORMS

By definition, remote sensing does not depend on the distance between the detected device and the object. Measurements can be conducted in the laboratory, at ground level in the field, from a drone or an unmanned aerial vehicle (UAV), aircrafts, and spacecrafts. Whatever the remote sensing device, they can be divided into four categories: point and image radiometers, and point and image spectrometers. *Radiometers* are *multispectral systems* that are characterized by several up to several tens of discrete broad bands with widths of tens to hundreds of nanometers (usually > 50 nm bandwidth). *Spectrometers*, however, are *hyperspectral systems* characterized by up to several hundred narrow bands, a few

nanometers each, which continuously spread along the spectrum (Schaepman 2009). *Point radiometers* and *point spectrometers* integrate the incoming radiation and create a single string of wavelengths vs. radiance or reflectance values. This type of instrument is usually applied in the field, sometime with accessories such as an *integrating sphere* for separating reflectance, transmittance, and absorbance spectra, or a *leaf clip* or a *contact probe* for minimizing environmental effects. *Image radiometers* and *image spectrometers* create a two-dimensional array (spatial domain) of spectral data (third dimension) for each band. The number of bands determines the fourth dimension of a spectral cube. Hyperspectral reflectance signatures have the advantage of quantitatively assessing vegetation and soil biochemistry properties (Ustin et al. 2004; Ben-Dor et al. 2009) (Subsection 2.8).

2.1 The Landsat program

The *Landsat* program, a joint U.S. National Aeronautics and Space Administration (NASA) and the Geological Survey (USGS) mission, has been operated in space since 1972, till now with eight satellites belonging to four generations of sensors. The first sensor generation, named the *Multispectral Scanner* (*MSS*), onboard Landsat 1, 2, and 3, is characterized by four spectral bands in the green, red, and NIR regions, an 80-m resolution, and 18 days revisit time. The second generation, named the *Thematic Mapper* (*TM*), onboard Landsat 4 and 5, has six spectral bands in the VIS-NIR-SWIR with a 30-m resolution and one TIR band with a 90-m resolution. The temporal resolution was improved to 16 days. The third generation, named the *Enhanced Thematic Mapper Plus* (*ETM+*), onboard Landsat 7, has an additional panchromatic band with a 15-m resolution and improved resolution of the TIR band to 60 m. Landsat 8 belongs to the fourth generation, with a payload of two sensors, the *Operational Land Imager* (*OLI*) and the *Thermal Infrared Sensor* (*TIRS*). The former has two additional bands in the blue and in the SWIR while the latter has two thermal detectors. By being the longest global observation program, referenced to the same coordinate system, with repetitive acquisition of high resolution multispectral data, the program has many scientific applications, including monitoring ecological essential variables and assessing land-cover and land-use status and changes over time for global climate research. The archived Landsat images are free (Gutman and Masek 2012).

2.2 The SPOT program

The *Satellite Pour l'Observation de la Terre* (*SPOT*) is a commercial moderate spatial resolution program for earth observation that was initiated and designed in France with some participation of Belgium and Sweden. The first satellite in the series was launched in 1986 carrying the *High Resolution Visible* (*HRV*) sensor. This band setting enabled mainly vegetation monitoring and mapping. Two independent HRV sensors onboard consisted of 3 multispectral bands at 20-m resolution and one panchromatic band at 10 m each. The nominal revisit time of the SPOT is 26 days, and the swath width is 60 km. However, the notable advantage of the SPOT system is the ability to tilt the satellite up to ±27 degrees off-nadir. By doing so, the system made it possible to create a digital elevation model, improving the temporal resolution (11 observing possibilities at 45º latitude and 7 at the equator), and increasing the swath width to 950 km. Since the SPOT is a commercial program that relies on advance tasking, it does not have a periodic image database. This is a drawback for change detection and time series analysis of any specific location. The first five satellites in the program were operated by the French space agency (Centre National d'études Spatiales, CNES). The payload of the later satellites was approved in terms of an additional SWIR band and a better spatial resolution. SPOT 4 and 5 stopped functioning in 2013 and 2015, respectively. SPOT 6 and 7 were launched in 2012 and 2014, respectively, and operated by Astrium, an aerospace manufacturer subsidiary of the European Aeronautic Defence and Space Company (EADS). Together with the two Pléiades space systems (Subsection 2.7.1), they form a constellation of four satellites, 90° apart from one another.

2.3 The NOAA-AVHRR program

The *Advanced Very High Resolution Radiometer* (AVHRR), onboard the National Oceanic and Atmospheric Administration's (NOAA's) Polar Orbiting Environmental Satellites (POES), is a broadband five-channel instrument (or six-channel depending on the model) in the VIS, NIR, SWIR, and TIR regions. A constellation of two satellites provide at least four image acquisitions per 24 hr for any location on the globe. Data are acquired in two formats: the *Local Area Coverage* (*LAC*) with the nominal 1.1-km spatial resolution at nadir and the *Global Area Coverage* (*GAC*) sampled and averaged onboard a satellite with the nominal 4-km spatial resolution. The primary applications of the AVHRR for the land are vegetation monitoring through vegetation indices (Subsection 3.1), albedo (Liang 2001) (Subsection 3.8), and extracting land surface temperature (Qin et al. 2001). Despite the two drawbacks of the sensor, specifically, drifts of the satellite orbit and of the channel calibration, the main advantage of the AVHRR series for terrestrial ecology is the long-term global archived dataset of images gathered since July 1982 (Gutman and Masek 2012).

2.4 The VEGETATION program

The *VEGETATION* instrument, onboard SPOT 4 and 5, was aimed at daily monitoring of terrestrial vegetation cover at regional to global scales, over a long time span, for developing models of the biosphere dynamics interacting with climate models (Saint 1994). The instrument, called the HRVIR, was characterized by four spectral bands in the blue, red, NIR, and SWIR, with a 2200-km swath width and a 1.15-km pixel size at nadir.

2.5 The MODIS program

The *Moderate Resolution Imaging Spectroradiometer* (*MODIS*) program comprises two similar instruments installed onboard the *Terra* and *Aqua* NASA's spacecrafts (Guenther et al. 2002). The former was launched in 1999 and the latter in 2002. Having a 2,330-km swath width, the two MODIS instruments are able to observe every point on earth four times in 24 hours (morning, afternoon, and night). MODIS has 36 discrete bands in pixel sizes of 250, 500, and 1,000 m, enabling a large number of land, ocean, and atmospheric applications. The environmental ones include the monitoring of large-scale biosphere dynamics in conjunction with the global carbon cycle and detecting the photosynthetic activity of land and marine plants in conjunction with greenhouse gases that are absorbed and used in plant productivity. Also worth mentioning is the ability to observe short-term events, such as dust storms, droughts, volcanic eruptions, floods, wildfires, and more. Following their policy, the NASA images are also free. Among the land archived products are surface reflectance, net and gross primary productivity, leaf area index and fractional photosynthetically active radiation, vegetation indices, land surface temperature and emissivity, bidirectional reflectance distribution function and albedo, and snow cover. Note that unlike the AVHRR, the MODIS data are well calibrated and thus useful for time-series studies such as vegetation phenology and more.

2.6 The Sentinel-2 program

Sentinel-2 belongs to the European Space Agency (ESA) and the European Commission (EC) multi-mission program called Copernicus (former the GMES program) (Drusch et al. 2012). It is a polar-orbiting, multispectral high-resolution imaging mission for land monitoring, including vegetation health, land-use and land-cover status and change, inland and coastal waters, and related features. Sentinel-2 is characterized by 13 bands in the VIS, NIR, and SWIR with 10, 20, and 60-m spatial resolutions within a 290-km swath width. Sentinel-2 is a constellation of two spacecrafts. The first was launched in June 2015, and the second launch is scheduled for the end of 2016. When both are in orbit, the revisit time will be five days under the same viewing angles. Data is free for all users.

2.7 High spatial resolution satellites

2.7.1 *Commercial satellites*

The high spatial resolution satellite era started in 1998 with the launch of *IKONOS*, the first commercial space system. Since then, the number of similar satellites has gradually increased, with all possessing basically the same characteristics with some variations and improvements throughout the years (Table 1). The multispectral bands are commonly used for a large variety of terrestrial applications, mostly connected with vegetation, while the *panchromatic band* is using for mapping and creating a digital elevation model (DEM) created from the stereo pairs.

Among the unique capabilities of these space systems are the panchromatic band at a higher resolution than the four multispectral bands (B, G, R, and NIR). The resolution of the multispectral bands is four times bigger than that of the panchromatic one, enabling pan-sharpening (Zhang 2004). This process aimed at merging the two resolutions to create a single high resolution color image. Since the spaceborne systems operate according to commercial goals, striving to maximize the number of potential attempts in a given time period, the systems also have the ability to tilt the satellite and to acquire, typically 30º, off-nadir images. Consequently, following an image tasking, the revisit time can be as low as one or two days. The main drawback of these spaceborne systems is that, unlike the broadband ones, they lack a fixed revisit time. New images for a specific location, within a confined area and under a predefined threshold of cloud cover, can be ordered from the vendor. Consequently, the acquisition cost is relatively high and only historical images exist in the archive.

2.7.2 *The VENμS program*

Among the high resolution satellites, the *Vegetation and Environmental New Micro Spacecraft* (*VENμS)* is an exception. VENμS is not a commercial mission but a scientific one. It is a joint venture of the Israeli Space Agency (ISA) and the French Centre National d'Etudes Spatiales (CNES). The satellite's launch is planned for late 2017. The overall aim of the VENμS scientific mission is to acquire frequent, high resolution, multispectral images of pre-selected sites of interest all around the world. In addition, the scientific mission is aimed at demonstrating the relevance of VENμS observation capabilities in the framework of the Copernicus Program. This program represents an effort to bring environmental and security data and information providers together with users, to better understand each other and to agree on how to make such information available to the people who need it. Copernicus will comprise a constellation of eight satellites; one of them, Sentinel-2 (Subsection 2.6), has similar and complementary spectral characteristics to the VENμS but with a coarser spatial resolution and longer revisit time.

During the VENμS mission, the satellite will fly in a near polar sun-synchronous orbit at 720 km in height and an inclination angle of 98.27º. The equator crossing time is planned to be at 10:30 AM, descending mode. The whole system can be tilted up to 30º off-nadir to enable imaging targets at up to 360 km on either side of the track and can also be tilted forward or backward to provide more flexibility in selecting the scientific sites, evaluating the radiometric effects of viewing angle, etc. This orbit configuration will result in a 27-km swath, a camera resolution of 5.3 m, and the capability to observe about 120-150 pre-selected ground sites with a high repetitiveness of two days, and always with exactly the same angular acquisition conditions and minimization of directional effects. The high observing frequency is essential for detecting the dynamics of vegetation growth and of the short duration of phenological stages, as well as the rapid temporal changes of water quality.

The satellite will carry the *VENμS Super-Spectral Camera* (VSSC) that offers a compromise on spectral resolution to attain a high signal-to-noise ratio (SNR) despite the small ground sampled distance (GSD) of 5.3 m. This is accomplished by having 12 narrow spectral bands, referred to as "superspectral" imaging, ranging from 415 nm to 910 nm and including four red-edge bands. The bands, varying in width from 40 nm down to 16 nm, were chosen to retrieve key information about vegetation, water, and atmosphere,

along with other features, and are carefully located within the atmospheric absorption regions of H_2O and O_2 (Figure 1). One of the bands, at 620 nm, is duplicated, and both bands are positioned at the extremes of the angular field in the scan direction. The 1.5° difference in look angle between these two will allow three-dimensional imaging that will enable the construction of a DEM of the earth surface and the assessment of cloud heights. Special attention was given to the detection of vegetation status as required by agronomists, foresters, and ecologists but the band, setting could also prove useful for water quality studies in coastal areas and inland water bodies.

A chain of four product levels will be available for the end-users:

- Level 0 is the basic archived product that consists of a single date and single viewing angle acquisition at a GSD of 5.3 m.
- Level 1 products are those from a single date and single viewing angle acquisition of the top of atmosphere reflectances with a subpixel multi-date registration (map projected) at a GSD of 5.3 m. A cloud mask at a coarse resolution will be associated with this product.
- Level 2 products consist of those from a single date and single viewing angle acquisition of surface reflectances after cloud masking and atmospheric correction for all spectral bands at a 10-m GSD. The algorithms used for Level 2 processing take advantage of the two-day revisit period with constant observation angles since most short-term variations of TOA reflectance are due to atmospheric variations. In addition, Level 2 includes a series of products derived from the reflectance data.
- Level 3 products are the same as Level 2, but consist of a10-day composite of a single date and single angle acquisition. The aim of the Level 3 products is to reduce the data volume for users and to deliver a composite of the same variables as in Level 2 after masking the clouds based on the cloud-free pixels of the Level 2 data gathered during a short period (7 to 10 days) at a GSD of 10 m.

As mentioned above, the VENµS mission is designed to observe about 120-150 pre-selected ground sites. In order to select these scientific sites, an international call for proposals was released in 2014. The selection will give high priority to sites that have long-term data that can be observed by the VENµS system, to the scientific merit of the proposal, and to the limitation of the mission (coverage, storage, etc.). The selected teams will receive, within one month after acquisition, the data they requested over one or several sites, free of charge. In most cases, the products will be provided for the entire mission duration. Levels 2 and 3 and possibly Level 1 products will be available three months after the acquisitions to any scientist who does not belong to a selected team.

2.8 Hyperspectral instruments

In contrast to multispectral scanners that provide information in distinct bands, hyperspectral instruments acquire data at many and contiguous spectral bands, enabling the creation of detailed spectral signatures of the detected object. Accordingly, hyperspectral data are associated with more quantitative analyses in the attempt to assess the nature of the material under study, such as chlorophyll, nitrogen, and lignin concentrations or water content in the case of vegetation biochemical properties (Goodenough et al. 2006). For assistance in this task, several spectral libraries of natural and human-made materials are provided by different agencies (e.g., http://speclab.cr.usgs.gov/spectral-lib.html; http://speclib.jpl.nasa.gov/).

As of today, most of the operational image spectrometers are onboard airborne platforms. The advantage of these systems is not only the ability to acquire data at a relatively high spatial resolution of about a meter (depending on the flight height), in addition to the high spectral resolution (of about 10 nm or less), but also the versatility to satisfy the user requirements in terms of timing and flight parameters. On the other hand, due to costs and logistics, the use of airborne system is limited and lacks the periodic repeating nature of the spaceborne systems (Asner and Heidebrecht 2003). The most common

hyperspectral airborne scanners are listed in Table 2. Most of them cover the VIS-NIR-SWIR regions and have been used for a large variety of remote sensing applications.

Since 2000, hyperspectral scanners have also been installed on spacecrafts. Currently, data are available from two operational hyperspectral systems, Hyperion on EO1 and CHRIS on PROBA. *Hyperion* is a full-range instrument (375-2576 nm), consisting of 242 bands at a bandwidth of approximately 10-nm *full-width at half maximum* (*FWHM*). The instrument's swath is 7.5 km, containing 256 columns (pixels) with a 30-m spatial resolution. The system was found to be suitable for retrieving geologic (mineralogical/lithological) information (Kruse et al. 2003), as well as for vegetation studies (Pignatti et al. 2009). Nevertheless, it is reported that the Hyperion data had drawbacks, such as relatively low SNR, spectral and spatial artifacts related to the array malfunction, and a significant smile effect (Dadon et al. 2010). The *Compact High Resolution Imaging Spectrometer* (*CHRIS*) acquires 13-km^2 scenes at a 17-m spatial resolution in 18 user-selected visible and near-infrared wavelengths and can be reconfigured to provide 63 spectral bands at a spatial resolution of about 34 m. This system also strives to collect *bidirectional reflectance distribution function* (*BRDF*) data for a better understanding of spectral reflectances and, consequently, was designed to observe the ground at up to five different viewing angles. Houborg et al. (2015) declared that "the need for an operational [spaceborne] hyperspectral mission to produce repeatable high resolution images for all terrestrial ecosystems has not been fulfilled." Despite the current technical problems and other limitations, several hyperspectral systems are planned to be operational in the near future (Buckingham and Staenz 2008). Table 3 lists the in-orbit, under construction, and forthcoming hyperspectral satellites along with their spectral characteristics.

3 SPECTRAL INDICES

Spectral indices are mathematical manipulations of two or more spectral bands (or spectral regions) to enhance the signal of the phenomenon under study for predicting ecosystem responses. Assuming that a multiband analysis would provide more information than a single one, reflectance values from the original input bands are converted into a single, dimensionless value. With respect to ecological research, spectral indices can be coarsely divided into vegetation indices (VIs), soil, and other environmental indices and further subdivided into broadband and narrowband remote sensing systems. While broadband indices are associated with multispectral systems, narrowband remote sensing is associated with hyperspectral sensors.

More than fifty different VIs are reported in the literature (Agapiou et al. 2012; Roberts et al. 2012; Stagakis et al. 2012), but only the key ones are presented in this Chapter in order to demonstrate their principle in conjunction with different applications.

3.1 Broadband vegetation indices

The most familiar spectral indices are the *vegetation indices* (*VIs)* that attempt to intensify the plant signals for assessing their state and dynamics along with their biophysical properties. Therefore, they are the most widely used spaceborne product for monitoring the ecosystem. The broadband VIs are generally used for assessing the structural properties of the terrestrial vegetation (Roberts et al. 2012) such as Leaf Area Index (LAI) (Wang et al. 2005), fractional vegetation cover (Bajocco et al. 2012), aboveground biomass (Wessels et al. 2006), the fraction of absorbed photosynthetically active radiation (fAPAR) (Fensholt et al. 2004), net primary productivity (NPP) (Schloss et al. 1999), foliar loss and damage (Vogelmann 1990), and more.

The earliest and the most fundamental VI is the *Simple Ratio* (*SR*), proposed by Jordan (1969):

$$SR = \rho_{NIR} / \rho_R \quad (1)$$

where ρ is the reflectance of the subscripted spectral band. The SR is based on the difference between the maximum absorption of radiation in the red band (due to the chlorophyll pigments) and the maximum reflection of radiation in the NIR band (due to the leaf cellular structure), and the fact that soil spectra, lacking these mechanisms, typically do not show such a dramatic spectral difference. Since the range of the SR values, from 0 to infinity, is considered as a drawback, the same bands were used for formulating the *Normalized Difference Vegetation Index* (*NDVI*) (Rouse et al. 1973; Tucker 1979):

$$NDVI = (\rho_{NIR} - \rho_R) / (\rho_{NIR} + \rho_R) \tag{2}$$

The NDVI values range from -1 to +1; thus, it is possible to distinguish between the positive values of vegetation (dense and healthy vegetation has relatively high NDVI values) and soil (which has relatively low NDVI values) and the negative values of clouds, snow, and water. Over the years, NDVI has turned out to be the most widely used VI.

Despite the extensive use of the NDVI and its various applications, several notable limitations of this index have been documented. These include (1) the sensitivity of the index to dark and/or wet soil backgrounds (Huete 1988); (2) less sensitivity ('saturation') of the index values in cases of high values of chlorophyll content, LAI, and biomass that indicate dense and multilayered canopies (Figure 2) (Buschmann and Nagel 1993); and (3) sensitivity to atmospheric influences (Holben 1986) since aerosol increases the apparent reflectance in the red band by scattering sunlight directly to the sensor and decreases, to a lesser degree, the reflectance in the NIR by absorption of sunlight. To overcome these drawbacks, several approved VIs were proposed. Among them is the *Soil Adjusted Vegetation Index* (*SAVI*) that is less sensitive to the soil background and approximate vegetation biophysical properties over a wide range of LAI values:

$$SAVI = \frac{\rho_{NIR} - \rho_R}{\rho_{NIR} + \rho_R + L}(1 + L) \tag{3}$$

where L, usually equal to 0.5, is the canopy background adjustment factor.

In order to defeat the scattering effects from aerosols suspended in the atmosphere, two VIs were proposed. The *Atmospherically Resistant Vegetation Index* (*ARVI*) (Kaufman and Tanre 1992):

$$ARVI = \frac{\rho_{NIR} - \rho_{RB}}{\rho_{NIR} + \rho_{RB}}$$
$$\rho_{RB} = \rho_R - \gamma(\rho_B - \rho_R) \tag{4}$$

and the *Atmospheric Free Vegetation Index* (*AFRI*) (Karnieli et al. 2001):

$$AFRI_{SWIR3} = (\rho_{NIR} - 0.5\rho_{SWIR3}) / (\rho_{NIR} + 0.5\rho_{SWIR3}) \ . \tag{5}$$

The resistance of the ARVI to atmospheric effects (in comparison to the NDVI) is accomplished by a self-correction process for the atmospheric effect on the red channel, using the difference in the radiance between the blue and the red channels to correct the radiance in the red channel. γ is equal to one. In the AFRI, the red band of the NDVI is substituted by half of the values in the SWIR3 region (2.1 µm~~,~~ ~~Subsection 5.3~~).

Finally, the *Enhanced Vegetation Index* (*EVI*) (Huete et al. 2002) was invented to optimize the vegetation signal with improved sensitivity in high biomass regions and improved vegetation monitoring while correcting for canopy background signals and reducing atmosphere influences.

$$EVI = \frac{\rho_{NIR} - \rho_R}{\rho_{NIR} + C_1\rho_R - C_2\rho_B + L} \times G \tag{6}$$

where the coefficients adopted in the EVI algorithm are L = 1, $C1$ = 6, $C2$ = 7.5, and G (gain factor) = 2.5.

3.2 Narrowband vegetation indices

As opposed to the primary use of broadband VIs, i.e., assessing the structural properties of terrestrial vegetation, narrowband VIs are aimed at resolving fine spectral features along with their optimal combination for estimating pigments. Narrowband indices, retrieved from hyperspectral data, are able to detect slight modifications in leaf bio-chemistry and thus to quantitatively improve the identification of the material under study.

3.3 The red-edge

The *red-edge* refers to the steep increase of vegetation reflectance values from the minimum reflectance (~10%) in the red band due to chlorophyll absorption and maximum reflectance (~50%) in the NIR band due to the leaf cellular structure. This transition spectral region occurs between 700 and 800 nm. Observations show that the red-edge moves towards the longer wavelengths during the vegetation growth stage, while moving towards the shorter wavelengths ("*blue shift"*) either during the senescence stage or during vegetation stress (Figure 3). Bearing in mind the "saturation" weakness of the NDVI, these shifts, although stretching along only several tens of nanometers, are much more sensitive and better correlated with biophysical variables such as chlorophyll (Baret et al. 1992), nitrogen (Tarpley et al. 2000), plant stress (Smith et al. 2004), fAPAR (Vina and Gitelson 2005), vegetation fraction (Vina and Gitelson 2005), and LAI (Herrmann et al. 2011).

Since the movement of the red-edge is horizontal, (i.e., along the wavelengths) rather than vertical (i.e., along the reflectance values), it is impossible to use standard VIs for correlating the biophysical variables with the red-edge shifts. Therefore, linear interpolation among several narrow bands, located along the red-edge, was proposed to calculate the midpoint, termed the *red-edge position* (λ_{rep}), between the red and the NIR regions (Guyot and Baret 1988):

$$\lambda_{rep} = 700 + 40((((\rho_{670} + \rho_{780}) / 2) - \rho_{700}) / (\rho_{740} - \rho_{700})) \tag{7}$$

This interpolation method was modified for adaptation to several spaceborne systems having at least four red-edge, although broad, bands, such as MERIS, Sentinel-2, and VENμS (Clevers et al. 2002; Herrmann et al. 2011). Since the red-edge position is mathematically defined as the inflection point between the positive and the negative slope of the curve, its location can also be calculated, in the case of hyperspectral data, by the first or second derivative of the spectrum (Smith et al. 2004):

$$\rho_i' = \frac{\rho_{i+1} - \rho_{i-1}}{\lambda_{i+1} - \lambda_{i-1}} \quad \left| 700 \le i \ge 800 \right. \tag{8}$$

$$\rho_i'' = \frac{\rho'_{i+1} - \rho'_{i-1}}{\lambda_{i+1} - \lambda_{i-1}} \quad \left| 700 \le i \ge 800 \right. \tag{9}$$

where i refers to a specific wavelength, typically between 700 and 800 nm. It is important to mention that the derivative method can result in two inflection points for the red-edge region (Zarco-Tejada et al. 2003). Notwithstanding the importance of the red-edge, only several multispectral spaceborne systems have the appropriate bands. These are the *MEdium Resolution Imaging Spectrometer* (MERIS), the Sentinel-2 (Subsection 2.6), and the VENμS (Subsection 2.7.2).

3.4 Biological pigments (chlorophylls, carotenoids, and anthocyanins)

Biological pigments indicate the physiological condition of plant leaves (Gitelson et al. 2006). Among others, *chlorophylls* (green pigments) constitute the main group of pigments. They are essential for the

photosynthetic activity of plants by absorbing radiation in the blue and red regions. The second group of pigments is the *carotenoids* (yellow pigments) that absorb radiation in the blue region to prevent damage to the photosynthetic systems. The third group is the *anthocyanins* (red pigments) that absorb radiation in the green region and protect leaves from excess light. The main pigments and the central location of their absorption features are summarized in Table 4.

Since each type of pigment is associated with a unique and narrow absorption feature along the VIS region, although some overlap exists, different hyperspectral indices were proposed to identify them and discriminate between them. One of the earliest was the *Photochemical Reflectance Index* (PRI) (Gamon et al. 1992):

$$PRI = (\rho_{550} - \rho_{531}) / (\rho_{550} - \rho_{531}) \tag{10}$$

which is a normalized difference index (NDVI-like) that uses two narrow reflectance bands at 531 nm and 550 nm. Another one is the *Chlorophyll Absorption in Reflectance Index* (*CARI*) (Kim 1994):

$$CARI = (\rho_{700} - \rho_{670}) - 0.2(\rho_{700} - \rho_{550}) \tag{11}$$

This index and its following ones employed three narrow bands; the maximum depth of the chlorophyll absorption is at 670 nm in comparison to its shoulders at 550 and 700 nm, where minimum absorption occurs.

The *Modified Chlorophyll Absorption in Reflectance Index* (*MCARI*) was proposed by Daughtry et al. (2000) for assessing corn chlorophyll concentration from leaf and canopy reflectance:

$$MCARI = [(\rho_{700} - \rho_{670}) - 0.2(\rho_{700} - \rho_{550})](\rho 700 / \rho 670) \tag{12}$$

The *Transformed Chlorophyll Absorption in Reflectance Index* (*TCARI*) was proposed by Haboudane et al. (2002) to show that the TCARI, applied to corn, is more sensitive to chlorophyll at a lower chlorophyll leaf content:

$$TCARI = 3\{[(\rho_{700} - \rho_{670}) - 0.2(\rho_{700} - \rho_{550})](\rho 700 / \rho 670)\} \tag{13}$$

The TCARI and the *Optimized Soil-Adjusted Vegetation Index* (*OSAVI*) were combined into one index, the *TCARI/OSAVI*, in order to reduce the soil background and improve the sensitivity to chlorophyll content. The OSAVI is similar to the SAVI (Huete 1988), with an optimized parameter L (= 0.16) for improving the reduction of the soil effect on the vegetation spectra in the case of aggregated pixels (Rondeaux et al. 1996):

$$OSAVI = \frac{1.16(\rho_{800} - \rho_{670})}{\rho_{800} + \rho_{670} + 0.16} \tag{14}$$

$$TCARI / OSAVI = \frac{3\{[(\rho_{700} - \rho_{670}) - 0.2(\rho_{700} - \rho_{550})](\rho 700 / \rho 670)\}}{\frac{1.16(\rho_{800} - \rho_{670})}{\rho_{800} + \rho_{670} + 0.16}} . \tag{15}$$

Numerous chlorophyll indices took advantage of the bands within the red-edge reflectance line (Subsection 3.3). The *Normalized Difference Red Edge* (NDRE) (Barnes et al. 2000) has a NDVI form but replaces its bands with a red-edge band at 720 nm and a reference band from the NIR plateau at 790 nm:

$$NDRE = (\rho_{790} - \rho_{720}) / (\rho_{790} + \rho_{720}) \tag{16}$$

Based on the NDRE and NDVI, the *Canopy Chlorophyll Content Index* (*CCCI*) is a two-dimensional index (Barnes et al. 2000):

$$CCCI = NDRE - NDRE_{\min} / NDRE_{\max} - NDRE_{\min} \quad (17)$$

By scatter plotting the NDVI and NDRE, the prediction of possible $NDRE_{MIN}$ and $NDRE_{MAX}$ values is performed, and the resultant values are used to obtain the CCCI.

Other conceptual three-band models were developed and examined by Gitelson et al. (2006) and Gitelson (2012) for relating either the green band or the red-edge band to the main pigments. The *Chlorophyll Index* (*Cll*):

$$ChlI_{green} = \rho_{NIR}(1/\rho_{540-560} - 1/\rho_{NIR}) = (\rho_{NIR}/\rho_{green}) - 1 \quad (18)$$

$$ChlI_{red-edge} = \rho_{NIR}(1/\rho_{690-725} - 1/\rho_{NIR}) = (\rho_{NIR}/\rho_{red-edge}) - 1 \quad (19)$$

The *Carotenoids Index* (*CrI*):

$$CrI_{green} \propto \rho_{NIR}(1/\rho_{510-520} - 1/\rho_{560-570}) \quad (20)$$

$$CrI_{red-edge} \propto \rho_{NIR}(1/\rho_{510-520} - 1/\rho_{690-710}) \quad (21)$$

The *Anthocyanins Index* (*AnI*):

$$AnI \propto \rho_{NIR}(1/\rho_{530-570} - 1/\rho_{690-710}) \quad (22)$$

3.5 Nutrients (nitrogen, potassium, and phosphorus)

Among the nutrients, *nitrogen* (*N*) is an essential element in plant growth and productivity, and thus crucial to numerous ecological processes. Several absorption features are listed in the literature along the SWIR region (Curran 1989). Spectral indices derived from handheld, airborne, and spaceborne spectrometers are used for assessing N content. The majority of them are based on indirect indicators, mostly chlorophyll content, which was proven to be physiologically linked to N content. Thus the above-listed chlorophyll indices, e.g., CARI, MCARI, TCARI, and TCARI/OSAVI, have also been frequently used for assessing nitrogen.

On the other hand, since the 1510 nm is directly related to nitrogen content, SWIR-based nitrogen indices were developed and implemented. The *Normalized Difference Nitrogen Index* (*NDNI*), proposed by Serrano et al. (2002), is a log10 transformed reflectance nitrogen index based on the absorption feature of nitrogen at 1510 nm and a reference band at 1680 nm:

$$NDNI = \frac{[\log 10(1/\rho_{1510}) - [\log 10(1/\rho_{1680})]}{[\log 10(1/\rho_{1510}) - [\log 10(1/\rho_{1680})]} \quad (23)$$

Herrmann (2010), who explored the performances of different indices with respect to N content, found that the firm advantage of SWIR-based indices lies in their ability to predict, and in their sensitivity to, this constituent. The best index, named the *Normalized Ratio Index* (NRI_{1510}), utilized the 1510 and 660 nm bands:

$$NRI_{1510} = (\rho_{1510} - \rho_{660}) / (\rho_{1510} + \rho_{660}) \quad (24)$$

The two other constituents, *potassium* (*K*) and *phosphorus* (*P*), are also important macronutrients required by plants after N. However, vegetation indices have shown very limited success for assessing K and P. Pimstein et al. (2011) conducted an experiment in order to assess P and K in wheat plants using indices

and a partial least squares-regression (PLS-R) (Subsection 4.1). The correlation coefficient (r) value found using a vegetation index based on a two-wavelength index (1645 and 1715 nm) was 0.73, and the value found using a PLS-R analysis of K content was 0.88. K appears in plants as an ion K+; therefore, it is not expected to be spectrally detected by its bonds. Pimstein et al. (2011) and Thulin et al. (2014) have shown that wavelengths that are highly related to K content mainly occur in the NIR and the SWIR since the K status is closely related to leaf structure and water regime, respectively. Studies exploring the spectral assessment of K content in *in vivo* plants have achieved less satisfactory results than studies examining the spectral assessment of K stress. P appears in plants in adenosine di- and tri-phosphates (ADP and ATP, respectively) and, therefore, is expected to be spectrally detected as a result of bonds with other elements. Since P affects plant development and conditions Homolova et al. (2013), it is assumed that the material itself is not identified. Mutanga and Kumar (2007) applied a neural network (Subsection 4.1) and concluded that integrating the red-edge and SWIR depth of absorption features are important for P content assessment in the African savanna. Homolova et al. (2013) presented studies analyzing spectral data but did not mention studies exploring P indices; they did mention, though, that there are no pronounced P absorption features. Therefore, the exploration of early nutrient stress identification by spectral means with a high spatial resolution is suggested, along with searching for alternative methods of nutrient concentration assessment.

3.6 Broadband vegetation water indices

Vegetation water content is another crucial variable for assessing the state and dynamics of the plants with respect to water stress, drought, climate change, fire-resistance, and more. *Water indices* (*WIs*) rely on the sensitivity of the SWIR bands (either 1.2 or 1.6 or 2.1 μm, denoted as SWIR1, SWIR2, and SWIR3, respectively) to leaf/canopy water content while assuming the relative stability of the NIR region to this variable. The higher the index value, the healthier the vegetation is. The *Moisture Stress Index* (*MSI*) (Hunt and Rock 1989) is the equivalent of the SR but is based on the NIR and SWIR2 bands:

$$MSI = \rho_{NIR} / \rho_{SWIR2} \tag{25}$$

Normalized versions of the same principle have used either the SWIR1 or the SWIR2 bands. The *Normalized Difference Infrared Index* (*NDII*) was proposed by Hardisky et al. (1983):

$$NDII = (\rho_{NIR} - \rho_{SWIR2}) / (\rho_{NIR} + \rho_{SWIR2}) \tag{26}$$

while the *Normalized Difference Water Index* (*NDWI*) was proposed by Gao (1996):

$$NDWI = (\rho_{NIR} - \rho_{SWIR1}) / (\rho_{NIR} + \rho_{SWIR1}) \tag{27}$$

3.7 Narrowband vegetation water stress indices

Hyperspectral signatures of water-stressed leaves are correlated to values of midday *leaf water potential* (ψ_l), *stomatal conductance* (*gs*), and *non-photochemical quenching* (*NPQ*) (Rapaport et al. 2015). It is shown that opposite reflectance trends at 5.3–5.5 μm and around 1.5 μm, associated with independent changes in photoprotective pigment contents and water availability, respectively, were indicative of stress-induced alterations in ψ_l, gs, and NPQ. Furthermore, combining the spectral responses at these VIs and SWIR regions yielded three normalized water balance indices that were superior to various widely used reflectance models in predicting physiological values at both the leaf and canopy levels.

The proposed *Leaf Water Potential Index* (*LWPI*):

$$LWPI = (\rho_{1490} - \rho_{531}) / (\rho_{1490} + \rho_{531}) \tag{28}$$

the *Stomatal Conductance Index (SCI)*:

$$SCI = (\rho_{1500} - \rho_{538}) / (\rho_{1500} + \rho_{538}) \quad (29)$$

and the *Non-Photochemical Quenching Index* (*NPQI*):

$$NPQI = (\rho_{1485} - \rho_{550}) / (\rho_{1485} + \rho_{550}) \quad (30)$$

3.8 Broadband abiotic and other indices

During the past few decades, it has been shown that soil spectra across the VIS–NIR–SWIR regions are characterized by significant chromophores (e.g., OH, Fe^{3+}, CO_3, and COOH) enabling the quantitative analysis of soil properties (Mathieu et al. 1998; Ben-Dor 2002; Ben-Dor et al. 2006). Consequently, broadband spectral indices have been used to characterize several soil minerals and properties. The following are several examples of soil indices. It should be noted that for detecting *soil moisture* (*SM*) the same broad SWIR bands are practically used as for assessing vegetation water content (Ben-Dor et al. 2009) (Subsection 3.6).

The *Brightness Index* (*BI*) quantifies the albedo over the VIS region (Zaady et al. 2007; Escadafal and Bacha 1996):

$$BI = \frac{\sqrt{\rho_B{}^2 + \rho_G{}^2 + \rho_R{}^2}}{3} \quad (31)$$

The *Coloration Index* (*ColI*) is sensitive to ferric oxides (Ben-Dor et al. 2006):

$$ColI = (\rho_R - \rho_G) / (\rho_R + \rho_G) \quad (32)$$

The *Redness Index* (*RI*) indicates hematite minerals (Ben-Dor et al. 2006):

$$RI = \rho_R{}^2 / (\rho_B * \rho_G{}^3) \quad (33)$$

The *Clay Minerals Ratio* (*CMS*) highlights hydrothermally altered rocks containing clay and alunite (Drury 1987):

$$CMR = \rho_{SWIR2} / \rho_{SWIR3} \quad (34)$$

The *Ferrous Minerals Ratio (FMR)* (Drury 1987):

$$FMR = \rho_{SWIR2} / \rho_{NIR} \quad (35)$$

The *Iron Oxide Ratio* (*IOR*) indicates hydrothermally altered rocks that were oxidized due to iron-bearing sulphides (Drury 1987):

$$IOR = \rho_R / \rho_B \quad (36)$$

The *Crust Index* (*CI*) aims at distinguishing between cyanobacteria-based crusty surfaces and the exposed substrate (e.g., bare sands) (Karnieli 1997):

$$CI = (\rho_R - \rho_B) / (\rho_R + \rho_B) \quad (37)$$

The CI takes advantage of a unique spectral feature of soil biogenic crust containing cyanobacteria. The special phycobilin pigment in cyanobacteria contributes to producing a relatively higher reflectance in the blue region than does the same type of substrate without biocrusts.

The *Normalized Different Snow Index* (*NDSI*) was developed in order to distinguish between snow and non-snow-covered areas (Salomonson and Appel 2004):

$$NDSI = (\rho_R - \rho_{SWIR2}) / (\rho_R + \rho_{SWIR2}) \tag{38}$$

The NDSI is based on the fact that snow reflectance is high in the VIS wavelengths and has low reflectance in the SWIR ones.

The *Normalized Burn Ratio (NBR)* has been use for detecting fire scars (Miller and Quayle 2015):

$$NBR = (\rho_{NIR} - \rho_{SWIR2}) / (\rho_{NIR} + \rho_{SWIR2}) \tag{39}$$

This index relies on the differences the NIR and the SWIR bands have between pre- and post-fire images, especially in forested landscapes.

3.9 Albedo

Broadband albedo is the ratio of the amount of electromagnetic radiation reflected by a surface to the amount of energy incident upon it. This is a unitless variable that is expressed as a fraction or percentage. Albedo may refer to the entire solar spectrum (0.3–4.5 μm) or merely to the visible portion (O.4–0.7 μm). Albedo is an important earth surface variable for understanding the transfer of energy and mass from the terrestrial ecosystems to the atmosphere (Roberts et al. 2012). Liang (2004) presents regression analysis products for calculating albedo for the following sensors:

$$\alpha_{LandsatTM/ETM+} = 0.356\alpha_1 + 0.13\alpha_3 + 0.373\alpha_4 + 0.085\alpha_5 + 0.072\alpha_7 \tag{40}$$

$$\alpha_{AVHRR} = -0.3376\alpha_1^2 - 0.22707\alpha_2^2 + 0.7074\alpha_1\alpha_2 + 0.2915\alpha_1 + 0.5256\alpha_2 \tag{41}$$

$$\alpha_{MODIS} = 0.160\alpha_1 + 0.291\alpha_2 + 0.243\alpha_3 + 0.116\alpha_4 + 0.112\alpha_5 + 0.081\alpha_7 \tag{42}$$

$$\alpha_{VEGETATION} = 0.3512\alpha_1 + 0.1629\alpha_2 + 0.3415\alpha_3 + 0.1651\alpha_4 \tag{43}$$

where α refers to planetary albedo at the top of atmosphere (TOA).

3.10 Soil organic matter (lignin, cellulose, and protein)

Soil organic matter (*SOM*) refers to the organic constituents in the soil. It includes undecayed plant and animal residues at various stages of decomposition, cells and tissues of soil organisms, and substances synthesized by soil organisms. It affects the soil quality through both its chemical and physical properties. In contrast to the chemical properties, and thus the spectra, of soils, rocks, and minerals that remain stable over the years, organic matter in soils varies over time (Ben Dor et al. 1997). Therefore, the SOM spectrum should be related to the soil stage, including fresh, dry, or decomposed litter, with respect to the temporal domain (Ilani et al. 2016). Several studies have suggested diagnostic absorption features for various SOM components, all within the SWIR region (Elvidge 1990; Curran et al. 1992; Ben Dor et al. 1997). Table 5 presents the major absorption features for *cellulose*, *lignin*, and *protein*.

Based on narrow spectral bands, the *Cellulose Absorption Index* (*CAI*) was introduced by Daughtry (2001):

$$CAI = 100\left[0.5\left(\rho_{2031} + \rho_{2211}\right) - \rho_{2101}\right] \tag{44}$$

and the *Normalized Difference Lignin Index (NDLI)* by Serrano et al. (2002):

$$NDLI = \frac{\left[\log\left(1/\rho_{1754}\right) - \log\left(1/\rho_{1680}\right)\right]}{\left[\log\left(1/\rho_{1754}\right) + \log\left(1/\rho_{1680}\right)\right]} \quad . \tag{45}$$

4 SPECTRAL ANALYSIS METHODS

4.1 Multivariate analysis

As mentioned earlier, hyperspectral data, which consist of hundreds of narrow spectral bands, create almost contiguous spectral information of the detected object and enable the quantitative assessment of vegetation and soil bio-physio-chemical properties. Such detailed information cannot be provided by multispectral data. Only a few properties (e.g., chlorophyll content, soil organic matter, etc.) are usually of interest in order to effectively determine and characterize the detected substrate. However, the multivariate nature of hyperspectral datasets is distinguished by strong multi-collinearity. Often, a relatively low number of training samples (predictees) contrasts with a large number of spectral bands (predictors) used by hyperspectral instruments (Atzberger et al. 2010). One of the most popular methods to conduct a regression analysis while coping with the collinearity of the hyperspectral data is the *Partial Least Squares-Regression* (*PLS-R*) technique, an advanced extension of multiple linear regression modeling. Unlike the latter, PLS-R is able to correlate collinear, noisy, and distribution-independent datasets, even when the number of predictors greatly exceeds the number of training samples (Wold et al. 2001; Hansen and Schjoerring 2003; Nguyen and Lee 2006; Thulin et al. 2014). In short, a large number of wavelengths is reduced to a smaller set of principal components, also called latent variables or factors; therefore PLS-R may be a useful exploratory and predictive tool when applied to a hyperspectral dataset. Hansen and Schjoerring (2003) showed that the PLS-R method improved the prediction of green biomass and leaf nitrogen concentration by lowering the root mean squared error (RMSE) when compared to the best examined narrow-band indices. Using PLS-R, predictive models that are better than traditional vegetation indices were created by Pimstein et al. (2007) for dry biomass, water content, and leaf area index, and by Pimstein et al. (2011) for predicting potassium and phosphorus contents in crop plants. Atzberger et al. (2010) demonstrated that the PLS-R method was superior to other methods, namely the stepwise multiple linear regression and principal component regression, for predicting total canopy chlorophyll content. Thulin (2014) successfully used this method to construct predictive models for estimating crude protein, digestibility, lignin, and cellulose concentration in temperate pastures. Paz-Kagan et al. (2014) found suitable PLS-R models for predicting soil properties including sand–silt–clay content, ammonium, nitrate, pH, residual water, soil organic matter, electric conductivity, potassium, phosphorus, potential active carbon, and hydraulic conductivity. Rozenstein et al. (2015) emphasized the importance of *pre-processing transformations (PPTs)* prior to the PLS-R analysis, such as *Savitzky–Golay smoothing*, *autoscale*, and/or *generalized least squares weighting*, that might approve the prediction. Choosing the best performing PPTs depends on the dataset and requires testing to ascertain an effective model.

Yet PLS-R is not the only method for modeling soil and vegetation properties using hyperspectral data. Other machine learning algorithms approaches, such as *support vector machines* (*SVM*), *artificial neural networks* (*ANN*), and *bayesian model averaging* (*BMA*), have been used to tackle regression problems, and to predict continuous variables. A review of SVM use in remote sensing is given by (Mountrakis et al. 2011). Durbha et al. (2007) used SVM regression for the retrieval of leaf area index from a multi-angle imaging spectroradiometer. Mirzaie at al. (2014) successfully used several approaches, including PLS-R and ANN, to predict vegetation water content using hyperspectral data. Zaho et al. (2013) estimated multiple foliage biochemical variables (including nitrogen, hydrogen, carbon, cellulose, lignin,

chlorophyll (a or b), carotenoid, polar and nonpolar extractives, leaf mass per area, and equivalent water thickness) from 27 spectral-chemical datasets using PLS-R and BMA. This arsenal of statistical learning tools keeps expanding with time, as new methods are adapted for use with hyperspectral data.

4.2 Multitemporal data processing

Several space programs have already been in orbit for more than 30 years (Gutman and Masek 2012). These programs are the Landsat that was started in 1972, NOAA-AVHRR in 1981, and SPOT in 1986 (see Section 2 for details). Several other programs are younger (e.g., VEGETATION and MODIS), have just launched (e.g., Sentinel-2), or will be launched in the near future (VENμS) in the attempt to provide images for many years to come. Although not all the programs have the same spectral characteristics and/or revisit time, the long-term time series of images have considerable potential for studying terrestrial ecology in terms of the land-cover dynamics. A distinction should be made between space programs that provide (nearly) daily data (e.g., AVHRR, MODIS, VEGETATION, Sentinel-2, VENμS) and those that provide periodic images (e.g., Landsat, SPOT). The former group is capable of providing a continuous time series of short-term changes, usually applied to vegetation indices. The temporal archive of AVHRR, sometime merged with the MODIS data, creates a long time series with statistically significant trends that may also be extended to other operated or future systems (Potter et al. 2005; Nemani et al. 2009; Karnieli et al. 2014). Several attempts have been conducted to compare NDVI datasets derived from different sensors, e.g., Landsat, SPOT, AVHRR, MODIS, VEGETATION, and others to construct a long-term NDVI time series (Fensholt and Sandholt 2005; Tucker et al. 2005; Brown et al. 2006; Ji et al. 2008). The latter group may provide data to conduct a change detection analysis between two or among several images, most likely to quantify inter-annual or intra-annual (seasonal) slow changes (e.g., Volcani et al. 2005; Karnieli et al. 2008; Karnieli et al. 2014). In this context, different change detection methods have been widely applied, such as *post-classification comparison*, *image/band/index rationing or differencing*, *change vector analysis*, and more (see review in Singh 1989; Mas 1999; Coppin et al. 2004; Lu et al. 2004). With respect to ecological monitoring, Willis (2015) classified the change detection applications into (1) uniform conversions between land-use and land-cover classes; (2) irregular variations such as disturbance; and (3) continuous fluctuations such as seasonal plant cycling.

4.3 Phenological studies

The term *phenology* is usually defined as "the study of the timing of recurring biological phases, the cause of their timing with regard to biotic and abiotic forces, and the interaction among phases of the same or different species" (Lieth 1976). With respect to climate change in conjunction with associate alterations of the growing season, the timing of phenological events has become a significant means for assessing the environmental implications of precipitation and temperature trends in a large variety of spatial scales– from individual plant species, through vegetation communities at regional, continental, and up to global scales. Traditionally, ground observations of vegetation have relied on monitoring key botanical events, namely green-up, blooming, maturity, senescence, and dormancy of specific species in a unique location such as a botanical garden (e.g., Yang and You-hao 2000). In contrast, remote sensing can upscale point and local observations and provide valuable digital data over vast areas and temporal scales at regular intervals using different environmental and climatic variables (Ganguly et al. 2010). Plant phenology modeling is a developing research field that may provide predictions of phenological cycles and their responses to climate change scenarios. In this regard, many different phenology models have been established in the last decades. These models range from simple to complex ones, depending on the species diversity, predictors, assumptions and their spatial scales. Curnel and Oger (2006) distinguished among several types of such techniques: threshold-based, derivatives, logistic curves, moving averages, and empirical equations. These models mostly use satellite vegetation indices (VIs) data in general, and NDVI, in particular. Spaceborne data enable the identification of several phenological indicators, including greenness onset, maturity onset, maximum greenness, and senescence onset and offset. These indicators are used for quantifying the start, end, and length of the growing season in a specific year.

Long-term repetitive data can be obtained from several spaceborne systems such as NOAA-AVHRR, MODIS, and the VEGETATION instrument (Section 2) that enable inter-annual variability in vegetation trends to be analyzed (de Jong et al. 2012).

4.4 Multi-source data fusion

The "*multi-concept*" was proposed during the early days of modern remote sensing (Simonett et al. 1983) with the understanding that merging data from different sources would provide more useful information, denoted hereafter as *multi-source*. The multi-concept includes multi-band, multi-sensor, multi-platform, multi-stage, multi-angle, multi-temporal, multi-(spatial, spectral, and radiometric) resolution, multi-phase, multi-polarization, and more. This concept still holds today and is intensively implemented by the leading space agencies, e.g., the USA's National Aeronautics and Space Administration (NASA) and the European Space Agency (ESA). Of special note is NASA's constellation, called the *A-track*, which consists of several Earth-observing satellites that follow each other seconds to minutes apart along the same orbital "track." Since each sensor has different characteristics, e.g., spectral bands, the constellation allows near-simultaneous observations of a wide variety of variables to aid the scientific community in advancing the knowledge of the Earth-system. The European Commission and ESA's *Copernicus* program, based on six different spaceborne sensors (Sentinel 1-6), aims at using multi-source data to get timely quality information on land, atmospheric, and oceanographic variables at a global scale. Such multi-source opportunities herald a new research era for remote sensing scientists in terms of methods and algorithms that, in turn, provide new and valuable data.

Recent studies have been carried out with a new trend of attempting to conduct data fusing between different spectral bands in order to enhance the image analysis or interpretation through the new product. Fusing the high-resolution panchromatic band and the multispectral bands for the purpose of creating a single high resolution color image was mentioned above (Subsection 2.7.1). Furthermore, fusions between the coarse spatial resolution and the high temporal resolution of the MODIS and the opposite spatial/temporal resolutions of the Landsat in the reflective bands were used for mapping forest disturbances (Hilker et al. 2009). The Landsat reflective bands, in conjunction with the MODIS thermal bands, were used for monitoring field-scale evapotranspiration (Kustas et al. 2003; Agam et al. 2007; Gao et al. 2012). The ability of hyperspectral systems to study the biophysical properties of vegetation and the ability of a *Light Detection And Ranging* (LiDAR) system to interpret the 3D vegetation structure at different levels (e.g., canopy and understory) have been cooperatively used for mapping and classifying forest areas (Mundt et al. 2006; Anderson et al. 2008; Dalponte et al. 2008). Microwave (radar) data in conjunction with reflective data were used for several applications such as extracting forest attributes (Treuhaft et al. 2004) and water areas (Hong et al. 2015). For these and for many other terrestrial ecological applications, such multi-source systems have been recently installed on light aircrafts, such as the *Airborne Observation Platform* (AOP) operated by the National Ecological Observatory Network (NEON) (Kampe et al. 2010), the *Carnegie Airborne Observatory-2* (CAO-2) operated by the Carnegie Institution for Science (Asner et al. 2012), and the *Goddard's LiDAR, Hyperspectral and Thermal* (G-LiHT) airborne imager operated by NASA (Cook et al. 2013).

5 INCORPORATING ECOLOGICAL VARIABLES WITH REMOTE SENSING

The Chapter summarizes the key ecological variables with respect to their analysis mean, main spectral bands, and the types of remote sensing platforms. It shows that remote sensing, spectroscopic methods, and related spectral analyses provide essential data for a variety of ecological studies and applications. Table 6 aims at synthesizing all the details, demonstrating the linkage between the ecosystem variables and/or ecological applications with their respective analysis means, the main applied spectral bands, and the most utilized remote system platform.

6 SUMMARY

The Chapter reviews remote sensing capabilities for terrestrial ecology and provides the readers with detailed information on remote sensing means, algorithms, and techniques. The document, which is written from a remote sensing perspective, presents a wide range of remote sensing analysis methods related to ecological applications. Nevertheless, despite the comprehensive and long-term link between the two disciplines, there are still fundamental challenges that must be overcome. Below are listed several steps that can be taken as derived from the Chapter:

- The fusion and integration between different instruments that acquire data in different parts of the electromagnetic spectrum, such as high spatial resolution optical, hyperspectral, radar, and LiDAR systems, would initiate new methods and algorithms, as well as incorporate them into ecological models in a wide range of spatial scales (Turner et al. 2004; Zhang 2010; Cook et al. 2013).
- The exploration of more diagnostic narrow bands, particularly in the red-edge and SWIR regions, would refine and improve the relationship between spectroscopic data and the biological, chemical, and physical properties of biotic and abiotic substrates.
- The development and implementation of advanced multivariant data analysis and image processing, such as machine learning algorithms, might improve the interpretation of hyperspectral data.
- Developments in the use of new remote sensing platforms, such as *unmanned aerial vehicles* (UAVs), commonly referred as drones, should continue. Compared to airborne and spaceborne systems, UAVs are more affordable, inexpensive, controllable, flexible in use, and reach a very high spatial resolution (~1 m). As the radiometers and spectrometers become lighter, they can be carried onboard UAVs and utilized in plot to local scale terrestrial ecology applications. Drones can also can be used to validate data from spaceborne missions (Panda et al. 2016).
- Remote sensing and physical models can be combined for terrestrial ecosystem applications since such models make a crucial contribution to the accurate determination of ecosystem properties and to the derivation of ecosystem information products (Goodenough et al. 2006; Baret 2016).

ACKNOWLEGEMENTS

The author wishes to thank Prof. Eyal Ben Dor, Dr. Agustin Pimstein, Dr. Ittai Herrmann, Dr. Offer Rozenstein, and Mr. Abraham Tal for their fruitful contributions.

REFERENCES

Agam, N., Kustas, W.P., Anderson, M.C., Li, F., & Neale, C.M.U. (2007). A vegetation index based technique for spatial sharpening of thermal imagery. *Remote Sensing of Environment,* **107**, 545-558.

Agapiou, A., Hadjimitsis, D.G., & Alexakis, D.D. (2012). Evaluation of Broadband and Narrowband Vegetation Indices for the Identification of Archaeological Crop Marks. *Remote Sensing,* **4**, 3892-3919.

Anderson, J.E., Plourde, L.C., Martin, M.E., Braswell, B.H., Smith, M.-L., Dubayah, R.O., Hofton, M.A., & Blair, J.B. (2008). Integrating waveform lidar with hyperspectral imagery for inventory of a northern temperate forest. *Remote Sensing of Environment,* **112**, 1856-1870.

Asner, G.P., & Heidebrecht, K.B. (2003). Imaging spectroscopy for desertification studies: Comparing AVIRIS and EO-1 Hyperion in Argentina drylands. *Ieee Transactions on Geoscience and Remote Sensing,* **41**, 1283-1296.

Asner, G.P., Knapp, D.E., Boardman, J., Green, R.O., Kennedy-Bowdoin, T., Eastwood, M., Martin, R.E., Anderson, C., & Field, C.B. (2012). Carnegie Airborne Observatory-2: Increasing science data dimensionality via high-fidelity multi-sensor fusion. *Remote Sensing of Environment,* **124**, 454-465.

Atzberger, C., Guerif, M., Baret, F., & Werner, W. (2010). Comparative analysis of three chemometric techniques for the spectroradiometric assessment of canopy chlorophyll content in winter wheat. *Computers and Electronics in Agriculture,* **73**, 165-173.

Bajocco, S., De Angelis, A., & Salvati, L. (2012). A satellite-based green index as a proxy for vegetation cover quality in a Mediterranean region. *Ecological Indicators,* **23**, 578-587.

Baret, F. (2016). Canopy biophysical variables retrieval from the inversion of reflectance models. In P.S. Thenkabail (Ed.), *Land Resources Monitoring, Modeling, and Mapping with Remote Sensing*. Boca Raton, FL: CRC Press, Taylor & Francis Group.

Baret, F., Jacquemoud, S., Guyot, G., & Leprieur, C. (1992). Modeled analysis of the biophysical nature of spectral shifts and comparison with information-content of broad bands. *Remote Sensing of Environment,* **41**, 133-142.

Barnes, E.M., Clarke, T.R., Richards, S.E., Colaizzi, P.D., Haberland, J., Kostrzewski, M., Waller, P., Choi, C., Riley, E., Thompson, T., Lascano, R.J., Li, H., & Moran, M.S. (2000). Coincident detection of crop water stress, nitrogen status and canopy density using ground-based multispectral data. In P.C. Robert, R.H. Rust & W.E. Larson (Eds.), *Proceedings of the 5th International Conference on Precision Agriculture* (pp. 1-15). Bloomington, MN: ASA-CSSA-SSSA.

Ben-Dor, E. (2002). Quantitative remote sensing of soil properties. In D.L. Sparks (Ed.), *Advances in Agronomy, Vol 75* (pp. 173-243)

Ben-Dor, E., Chabrillat, S., Dematte, J.A.M., Taylor, G.R., Hill, J., Whiting, M.L., & Sommer, S. (2009). Using Imaging Spectroscopy to study soil properties. *Remote Sensing of Environment,* **113**, S38-S55.

Ben-Dor, E., Levin, N., Singer, A., Karnieli, A., Braun, O., & Kidron, G.J. (2006). Quantitative mapping of the soil rubification process on sand dunes using an airborne hyperspectral sensor. *Geoderma,* **131**, 1-21.

Ben Dor, E., Inbar, Y., & Chen, Y. (1997). The reflectance spectra of organic matter in the visible near-infrared and short wave infrared region (400-2500 nm) during a controlled decomposition process. *Remote Sensing of Environment,* **61**, 1-15.

Brown, M.E., Pinzon, J.E., Didan, K., T Morisette, J., & Tucker, C.J. (2006). Evaluation of the consistency of long-term NDVI time series derived from AVHRR, SPOT-Vegetation, SeaWiFS, MODIS, and Landsat ETM+ sensors. *Ieee Transactions on Geoscience and Remote Sensing,* **44**, 1787-1793.

Buckingham, R., & Staenz, K. (2008). Review of current and planned civilian space hyperspectral sensors for EO. *Canadian Journal of Remote Sensing,* **34**, S187-S197.

Buschmann, C., & Nagel, E. (1993). Invivo spectroscopy and internal optics of leaves as basis for remote-sensing of vegetation. *International Journal of Remote Sensing,* **14**, 711-722.

Clevers, J., De Jong, S.M., Epema, G.F., Van der Meer, F.D., Bakker, W.H., Skidmore, A.K., & Scholte, K.H. (2002). Derivation of the red edge index using the MERIS standard band setting. *International Journal of Remote Sensing,* **23**, 3169-3184.

Cook, B.D., Corp, L.A., Nelson, R.F., Middleton, E.M., Morton, D.C., McCorkel, J.T., Masek, J.G., Ranson, K.J., Ly, V., & Montesano, P.M. (2013). NASA Goddard's LiDAR, Hyperspectral and Thermal (G-LiHT) Airborne Imager. *Remote Sensing,* **5**, 4045-4066.

Coppin, P., Jonckheere, I., Nackaerts, K., Muys, B., & Lambin, E. (2004). Digital change detection methods in ecosystem monitoring: a review. *International Journal of Remote Sensing,* **25**, 1565-1596.

Curnel, Y., & Oger, R. (2006). Agrophenology indicators from remote sensing: State of the art. In B. Baruth, A. Royer & G. G. (Eds.), *Remote Sensing Support to Crop Yield Forecast and Area Estimates* (pp. 31-38). Stresa, Italy: ISPRS.

Curran, P.J. (1989). Remote-sensing of foliar chemistry. *Remote Sensing of Environment,* **30**, 271-278.

Curran, P.J., Dungan, J.L., Macler, B.A., Plummer, S.E., & Peterson, D.L. (1992). Reflectance spectroscopy of fresh whole leaves for the estimation of chemical concentration. *Remote Sensing of Environment,* **39**, 153-166.

Dadon, A., Ben-Dor, E., & Karnieli, A. (2010). Use of Derivative Calculations and Minimum Noise Fraction Transform for Detecting and Correcting the Spectral Curvature Effect (Smile) in Hyperion Images. *Ieee Transactions on Geoscience and Remote Sensing,* **48**, 2603-2612.

Dalponte, M., Bruzzone, L., & Gianelle, D. (2008). Fusion of hyperspectral and LIDAR remote sensing data for classification of complex forest areas. *Ieee Transactions on Geoscience and Remote Sensing,* **46**, 1416-1427.

Daughtry, C.S.T. (2001). Discriminating crop residues from soil by shortwave infrared reflectance. *Agronomy Journal,* **93**, 125-131.

Daughtry, C.S.T., Walthall, C.L., Kim, M.S., de Colstoun, E.B., & McMurtrey, J.E. (2000). Estimating corn leaf chlorophyll concentration from leaf and canopy reflectance. *Remote Sensing of Environment,* **74**, 229-239.

de Jong, R., Verbesselt, J., Schaepman, M.E., & de Bruin, S. (2012). Trend changes in global greening and browning: contribution of short-term trends to longer-term change. *Global Change Biology,* **18**, 642-655.

Drury, S. (1987). *Image Interpretation in Geology*. London: Allen and Unwin.

Drusch, M., Del Bello, U., Carlier, S., Colin, O., Fernandez, V., Gascon, F., Hoersch, B., Isola, C., Laberinti, P., Martimort, P., Meygret, A., Spoto, F., Sy, O., Marchese, F., & Bargellini, P. (2012). Sentinel-2: ESA's Optical High-Resolution Mission for GMES Operational Services. *Remote Sensing of Environment,* **120**, 25-36.

Durbha, S.S., King, R.L., & Younan, N.H. (2007). Support vector machines regression for retrieval of leaf area index from multiangle imaging spectroradiometer. *Remote Sensing of Environment,* **107**, 348-361.

Elvidge, C.D. (1990). Visible and near-infrared reflectance characteristics of dry plant materials. *International Journal of Remote Sensing,* **11**, 1775-1795.

Escadafal, R., & Bacha, S. (1996). Strategy for the dynamic study of desertification. In R. Escadafal, M.A. Mulders & L. Thiombiano (Eds.), *Monitoring Soils in the Environment with Remote Sensing and GIS* (pp. 19-34). Ouagadougou, Burkino Faso: Orstom editions.

Fensholt, R., & Sandholt, I. (2005). Evaluation of MODIS and NOAA AVHRR vegetation indices with in situ measurements in a semi-arid environment. *International Journal of Remote Sensing,* **26**, 2561-2594.

Fensholt, R., Sandholt, I., & Rasmussen, M.S. (2004). Evaluation of MODIS LAI, fAPAR and the relation between fAPAR and NDVI in a semi-arid environment using in situ measurements. *Remote Sensing of Environment,* **91**, 490-507.

Gamon, J.A., Penuelas, J., & Field, C.B. (1992). A NARROW-WAVEBAND SPECTRAL INDEX THAT TRACKS DIURNAL CHANGES IN PHOTOSYNTHETIC EFFICIENCY. *Remote Sensing of Environment,* **41**, 35-44.

Ganguly, S., Friedl, M.A., Tan, B., Zhang, X., & Verma, M. (2010). Land surface phenology from MODIS: Characterization of the Collection 5 global land cover dynamics product. *Remote Sensing of Environment,* **114**, 1805-1816.

Gao, B.C. (1996). NDWI - A normalized difference water index for remote sensing of vegetation liquid water from space. *Remote Sensing of Environment,* **58**, 257-266.

Gao, F., Kustas, W.P., & Anderson, M.C. (2012). A Data Mining Approach for Sharpening Thermal Satellite Imagery over Land. *Remote Sensing,* **4**, 3287-3319.

Gitelson, A.A. (2012). Nondestructive estimation of foliar pigment (chlorophylls, carotenoids, and anthocyanins) contents: Evaluating a semianalytical three-band model. In P.S. Thenkabail, J.G. Lyon & A. Huete (Eds.), *Hyperspectral Remote Sensing of Vegetation* (pp. 141-165). Boca Raton, FL: CRC Press.

Gitelson, A.A., Keydan, G.P., & Merzlyak, M.N. (2006). Three-band model for noninvasive estimation of chlorophyll, carotenoids, and anthocyanin contents in higher plant leaves. *Geophysical Research Letters,* **33**

Goodenough, D.G., Li, J.Y., Asner, G.P., Schaepman, M.E., Ustin, S.L., Dyk, A., & Ieee (2006). Combining hyperspectral remote sensing and physical modeling for applications in land ecosystems. *2006 Ieee International Geoscience and Remote Sensing Symposium, Vols 1-8* (pp. 2000-2004)

Guenther, B., Xiong, X., Salomonson, V.V., Barnes, W.L., & Young, J. (2002). On-orbit performance of the Earth Observing System Moderate Resolution Imaging Spectroradiometer; first year of data. *Remote Sensing of Environment,* **83**, 16-30.

Gutman, G., & Masek, J.G. (2012). Long-term time series of the Earth's land-surface observations from space. *International Journal of Remote Sensing,* **33**, 4700-4719.

Guyot, G., & Baret, F. (1988). Utilisation de la haute resolution spectrale pour suivre l'etat des couverts vegetaux. In, *4th International Colloquium "Spectral signatures of objects in remote sensing"* (pp. 279-286)

Haboudane, D., Miller, J.R., Tremblay, N., Zarco-Tejada, P.J., & Dextraze, L. (2002). Integrated narrow-band vegetation indices for prediction of crop chlorophyll content for application to precision agriculture. *Remote Sensing of Environment,* **81**, 416-426.

Hansen, P.M., & Schjoerring, J.K. (2003). Reflectance measurement of canopy biomass and nitrogen status in wheat crops using normalized difference vegetation indices and partial least squares regression. *Remote Sensing of Environment,* **86**, 542-553.

Hardisky, M.A., Klemas, V., & Smart, R.M. (1983). The influence of soil-salinity, growth form, and leaf moisture on the spectral radiance of spartina-alterniflora canopies. *Photogrammetric Engineering and Remote Sensing,* **49**, 77-83.

Herrmann, I., Karnieli, A., Bonfil, D.J., Cohen, Y., & Alchanatis, V. (2010). SWIR-based spectral indices for assessing nitrogen content in potato fields. *International Journal of Remote Sensing,* **31**, 5127-5143.

Herrmann, I., Pimstein, A., Karnieli, A., Cohen, Y., Alchanatis, V., & Bonfil, D.J. (2011). LAI assessment of wheat and potato crops by VEN mu S and Sentinel-2 bands. *Remote Sensing of Environment,* **115**, 2141-2151.

Hilker, T., Wulder, M.A., Coops, N.C., Linke, J., McDermid, G., Masek, J.G., Gao, F., & White, J.C. (2009). A new data fusion model for high spatial- and temporal-resolution mapping of forest disturbance based on Landsat and MODIS. *Remote Sensing of Environment,* **113**, 1613-1627.

Holben, B.N. (1986). Characteristics of maximum-value composite images from temporal avhrr data. *International Journal of Remote Sensing,* **7**, 1417-1434.

Homolova, L., Maenovsky, Z., Clevers, J.G.P.W., Garcia-Santos, G., & Schaeprnan, M.E. (2013). Review of optical-based remote sensing for plant trait mapping. *Ecological Complexity,* **15**, 1-16.

Hong, S., Jang, H., Kim, N., & Sohn, H.-G. (2015). Water Area Extraction Using RADARSAT SAR Imagery Combined with Landsat Imagery and Terrain Information. *Sensors,* **15**, 6652-6667.

Houborg, R., Fisher, J.B., & Skidmore, A.K. (2015). Advances in remote sensing of vegetation function and traits. *International Journal of Applied Earth Observation and Geoinformation,* **43**, 1-6.

Huete, A., Didan, K., Miura, T., Rodriguez, E.P., Gao, X., & Ferreira, L.G. (2002). Overview of the radiometric and biophysical performance of the MODIS vegetation indices. *Remote Sensing of Environment,* **83**, 195-213.

Huete, A.R. (1988). A Soil-Adjusted Vegetation Index (SAVI). *Remote Sensing of Environment,* **25**, 295-309.

Hunt, E.R., & Rock, B.N. (1989). etection of changes in leaf water-content using near-infrared and middle-infrared reflectances. *Remote Sensing of Environment,* **30**, 43-54.

Ilani, T., Herrmann, I., Karnieli, A., & Arye, G. (2016). Characterization of the biosolids composting process by hyperspectral analysis. *Waste management (New York, N.Y.),* **48**, 106-114.

Ji, L., Gallo, K., Eidenshink, J.C., & Dwyer, J. (2008). Agreement evaluation of AVHRR and MODIS 16-day composite NDVI data sets. *International Journal of Remote Sensing,* **29**, 4839-4861.

Jordan, C.F. (1969). Derivation of leaf-area index from quality of light on forest floor. *Ecology,* **50**, 663-&.

Kampe, T.U., Johnson, B.R., Kuester, M., & Keller, M. (2010). NEON: the first continental-scale ecological observatory with airborne remote sensing of vegetation canopy biochemistry and structure. *Journal of Applied Remote Sensing,* **4**

Karnieli, A. (1997). Development and implementation of spectral crust index over dune sands. *International Journal of Remote Sensing,* **18**, 1207-1220.

Karnieli, A., Gilad, U., Ponzet, M., Svoray, T., Mirzadinov, R., & Fedorina, O. (2008). Assessing land-cover change and degradation in the Central Asian deserts using satellite image processing and geostatistical methods. *Journal of Arid Environments,* **72**, 2093-2105.

Karnieli, A., Kaufman, Y.J., Remer, L., & Wald, A. (2001). AFRI - aerosol free vegetation index. *Remote Sensing of Environment,* **77**, 10-21.

Karnieli, A., Qin, Z., Wu, B., Panov, N., & Yan, F. (2014). Spatio-Temporal Dynamics of Land-Use and Land-Cover in the Mu Us Sandy Land, China, Using the Change Vector Analysis Technique. *Remote Sensing,* **6**, 9316-9339.

Kaufman, Y.J., & Tanre, D. (1992). Atmospherically Resistant Vegetation Index (ARVI) for EOS-MODIS. *Ieee Transactions on Geoscience and Remote Sensing,* **30**, 261-270.

Kim, M.S. (1994). The use of narrow spectral bands for improving remote sensing estimation of fractionally absorbed photosynthetically active radiation (fAPAR). In, *Department of Geography*. College Park, MD: University of Maryland.

Kruse, F.A., Boardman, J.W., & Huntington, J.F. (2003). Comparison of airborne hyperspectral data and EO-1 Hyperion for mineral mapping. *Ieee Transactions on Geoscience and Remote Sensing,* **41**, 1388-1400.

Kustas, W.P., Norman, J.M., Anderson, M.C., & French, A.N. (2003). Estimating subpixel surface temperatures and energy fluxes from the vegetation index-radiometric temperature relationship. *Remote Sensing of Environment,* **85**, 429-440.

Liang, S. (2004). *Quntative Remote Sensing of Land Surfaces*. Hoboken, NJ: John Wiley & Sons, Inc.

Liang, S.L. (2001). Narrowband to broadband conversions of land surface albedo I Algorithms. *Remote Sensing of Environment,* **76**, 213-238.

Lieth, H.H. (1976). Contributions to phenology seasonality research. *International Journal of Biometeorology,* **20**, 197-199.

Lu, D., Mausel, P., Brondizio, E., & Moran, E. (2004). Change detection techniques. *International Journal of Remote Sensing,* **25**, 2365-2407.

Mas, J.F. (1999). Monitoring land-cover changes: a comparison of change detection techniques. *International Journal of Remote Sensing,* **20**, 139-152.

Mathieu, R., Pouget, M., Cervelle, B., & Escadafal, R. (1998). Relationships between satellite-based radiometric indices simulated using laboratory reflectance data and typic soil color of an arid environment. *Remote Sensing of Environment,* **66**, 17-28.

Miller, J.D., & Quayle, B. (2015). Calibration and validation of immediate post-fire satellite-derived data to three severity metrics. *Fire Ecology,* **11**, 12-30.

Mirzaie, M., Darvishzadeh, R., Shakiba, A., Matkan, A.A., Atzberger, C., & Skidmore, A. (2014). Comparative analysis of different uni- and multi-variate methods for estimation of vegetation water content using hyper-spectral measurements (vol 26, pg 1, 2014). *International Journal of Applied Earth Observation and Geoinformation,* **28**, 260-260.

Mountrakis, G., Im, J., & Ogole, C. (2011). Support vector machines in remote sensing: A review. *Isprs Journal of Photogrammetry and Remote Sensing,* **66**, 247-259.

Mundt, J.T., Streutker, D.R., & Glenn, N.F. (2006). Mapping sagebrush distribution using fusion of hyperspectral and lidar classifications. *Photogrammetric Engineering and Remote Sensing,* **72**, 47-54.

Mutanga, O., & Kumar, L. (2007). Estimating and mapping grass phosphorus concentration in an African savanna using hyperspectral image data. *International Journal of Remote Sensing,* **28**, 4897-4911.

Nemani, R., Hashimoto, H., Votava, P., Melton, F., Wang, W., Michaelis, A., Mutch, L., Milesi, C., Hiatt, S., & White, M. (2009). Monitoring and forecasting ecosystem dynamics using the Terrestrial Observation and Prediction System (TOPS). *Remote Sensing of Environment,* **113**, 1497-1509.

Nguyen, H.T., & Lee, B.W. (2006). Assessment of rice leaf growth and nitrogen status by hyperspectral canopy reflectance and partial least square regression. *European Journal of Agronomy,* **24**, 349-356.

Panda, S.S., Rao, M.N., Thenkabail, P.S., & Fitzerald, J.E. (2016). Satellites and sensors from different eras and their characteristics. In P.S. Thenkabail (Ed.), *Remotely sensed data characterization, classification, and accuracies*. Boca Raton, FL: CRC Press, Taylor & Francis Group.

Paz-Kagan, T., Shachak, M., Zaady, E., & Karnieli, A. (2014). A spectral soil quality index (SSQI) for characterizing soil function in areas of changed land use. *Geoderma,* **230**, 171-184.

Pignatti, S., Cavalli, R.M., Cuomo, V., Fusilli, L., Pascucci, S., Poscolieri, M., & Santini, F. (2009). Evaluating Hyperion capability for land cover mapping in a fragmented ecosystem: Pollino National Park, Italy. *Remote Sensing of Environment,* **113**, 622-634.

Pimstein, A., Karnieli, A., Bansal, S.K., & Bonfil, D.J. (2011). Exploring remotely sensed technologies for monitoring wheat potassium and phosphorus using field spectroscopy. *Field Crops Research,* **121**, 125-135.

Pimstein, A., Karnieli, A., & Bonfil, D.J. (2007). Wheat and maize monitoring based on ground spectral measurements and multivariate data analysis. *Journal of Applied Remote Sensing,* **1.**

Plummer, S.E. (2000). Perspectives on combining ecological process models and remotely sensed data. *Ecological Modelling,* **129**, 169-186.

Potter, C., Tan, P.N., Kumar, V., Kucharik, C., Klooster, S., Genovese, V., Cohen, W., & Healey, S. (2005). Recent history of large-scale ecosystem disturbances in North America derived from the AVHRR satellite record. *Ecosystems,* **8**, 808-824.

Qin, Z.H., Dall'Olmo, G., Karnieli, A., & Berliner, P. (2001). Derivation of split window algorithm and its sensitivity analysis for retrieving land surface temperature from NOAA-advanced very high resolution radiometer data. *Journal of Geophysical Research-Atmospheres,* **106**, 22655-22670.

Rapaport, T., Hochberg, U., Shoshany, M., Karnieli, A., & Rachmilevitch, S. (2015). Combining leaf physiology, hyperspectral imaging and partial least squares-regression (PLS-R) for grapevine water status assessment. *Isprs Journal of Photogrammetry and Remote Sensing,* **109**, 88-97.

Roberts, A.D., Roth, L.K., & Perroy, L.R. (2012). Hyperspectral Vvgetation indices. In P.S. Thenkabail, J.G. Lyon & A. Huete (Eds.), *Hyperspectral Remote Sensing of Vegetation* (pp. 309-328). Boca Raton, FL: CRC Press.

Rondeaux, G., Steven, M., & Baret, F. (1996). Optimization of soil-adjusted vegetation indices. *Remote Sensing of Environment,* **55**, 95-107.

Rouse, J.W., Haas, R.H., Schell, J.A., & Deering, D.W. (1973). Monitoring vegetation systems in the Great Plains with ERTS. In S.C. Freden, E.P. Mercant & M.A. Becker (Eds.), *Third Earth Resources Technology Satellite-1 Symposium* (pp. 309-317). Washington, D.C.: NASA.

Rozenstein, O., Paz-Kagan, T., Salbach, C., & Karnieli, A. (2015). Comparing the Effect of Preprocessing Transformations on Methods of Land-Use Classification Derived From Spectral Soil Measurements. *Ieee Journal of Selected Topics in Applied Earth Observations and Remote Sensing,* **8**, 2393-2404.

Saint, G. (1994). "VEGETATION" onboard SPOT 4 mission specification. In. ISPRA, Italy

Salomonson, V.V., & Appel, I. (2004). Estimating fractional snow cover from MODIS using the normalized difference snow index. *Remote Sensing of Environment,* **89**, 351-360.

Schaepman, M.E. (2009). Imaging spectrometers. In T.A. Warner, M. Duane Nellis & G.M. Foody (Eds.), *The SAGE Handbook of Remote Sensing* (pp. 166-178). London, UK: SAGE Publications Ltd.

Schloss, A.L., Kicklighter, D.W., Kaduk, J., Wittenberg, U., & Participants Potsdam, N.P.P.M.I. (1999). Comparing global models of terrestrial net primary productivity (NPP): comparison of NPP to climate and the Normalized Difference Vegetation Index (NDVI). *Global Change Biology,* **5**, 25-34.

Serrano, L., Penuelas, J., & Ustin, S.L. (2002). Remote sensing of nitrogen and lignin in Mediterranean vegetation from AVIRIS data: Decomposing biochemical from structural signals. *Remote Sensing of Environment,* **81**, 355-364.

Simonett, D.S., Green, R.G., Reeves, G., Estes, J.E., Bertke, S.E., & Sailer, C.T. (1983). The development and principles of remote sensing. *Manual of Remote Sening*. Falls Church, VA.: Ameican Society of Photogrammetry.

Singh, A. (1989). DIGITAL CHANGE DETECTION TECHNIQUES USING REMOTELY-SENSED DATA. *International Journal of Remote Sensing,* **10**, 989-1003.

Smith, K.L., Steven, M.D., & Colls, J.J. (2004). Use of hyperspectral derivative ratios in the red-edge region to identify plant stress responses to gas leaks. *Remote Sensing of Environment,* **92**, 207-217.

Stagakis, S., Gonzalez-Dugo, V., Cid, P., Guillen-Climent, M.L., & Zarco-Tejada, P.J. (2012). Monitoring water stress and fruit quality in an orange orchard under regulated deficit irrigation using narrow-band structural and physiological remote sensing indices. *Isprs Journal of Photogrammetry and Remote Sensing,* **71**, 47-61.

Tarpley, L., Reddy, K.R., & Sassenrath-Cole, G.F. (2000). Reflectance indices with precision and accuracy in predicting cotton leaf nitrogen concentration. *Crop Science,* **40**, 1814-1819.

Thulin, S., Hill, M., Held, A., Jones, S., & Woodgate, P. (2014). Predicting levels of crude protein, digestibility, lignin and cellulose in temperate pastures using hyperspectral image data. *American Journal of Plant Sciences,* **5**, 997-1019.

Treuhaft, R.N., Law, B.E., & Asner, G.P. (2004). Forest attributes from radar interferometric structure and its fusion with optical remote sensing. *Bioscience,* **54**, 561-571.

Tucker, C.J. (1979). Red and photographic infrared linear combinations for monitoring vegetation. *Remote Sensing of Environment,* **8**, 127-150.

Tucker, C.J., Pinzon, J.E., Brown, M.E., Slayback, D.A., Pak, E.W., Mahoney, R., Vermote, E.F., & El Saleous, N. (2005). An extended AVHRR 8-km NDVI dataset compatible with MODIS and SPOT vegetation NDVI data. *International Journal of Remote Sensing,* **26**, 4485-4498.

Turner, D.P., Ollinger, S.V., & Kimball, J.S. (2004). Integrating remote sensing and ecosystem process models for landscape- to regional-scale analysis of the carbon cycle. *Bioscience,* **54**, 573-584.

Ustin, S.L., Roberts, D.A., Gamon, J.A., Asner, G.P., & Green, R.O. (2004). Using imaging spectroscopy to study ecosystem processes and properties. *Bioscience,* **54**, 523-534.

Vina, A., & Gitelson, A.A. (2005). New developments in the remote estimation of the fraction of absorbed photosynthetically active radiation in crops. *Geophysical Research Letters,* **32**

Vogelmann, J.E. (1990). Comparison between 2 vegetation indexes for measuring different types of forest damage in the north-eastern United-States. *International Journal of Remote Sensing,* **11**, 2281-2297.

Volcani, A., Karnieli, A., & Svoray, T. (2005). The use of remote sensing and GIS for spatio-temporal analysis of the physiological state of a semi-arid forest with respect to drought years. *Forest Ecology and Management,* **215**, 239-250.

Wang, Q., Adiku, S., Tenhunen, J., & Granier, A. (2005). On the relationship of NDVI with leaf area index in a deciduous forest site. *Remote Sensing of Environment,* **94**, 244-255.

Wessels, K.J., Prince, S.D., Zambatis, N., Macfadyen, S., Frost, P.E., & Van Zyl, D. (2006). Relationship between herbaceous biomass and 1-km(2) Advanced Very High Resolution Radiometer (AVHRR) NDVI in Kruger National Park, South Africa. *International Journal of Remote Sensing,* **27**, 951-973.

Willis, K.S. (2015). Remote sensing change detection for ecological monitoring in United States protected areas. *Biological Conservation,* **182**, 233-242.

Wold, S., Sjostrom, M., & Eriksson, L. (2001). PLS-regression: a basic tool of chemometrics. *Chemometrics and Intelligent Laboratory Systems,* **58**, 109-130.

Yang, Z.-h., & You-hao, E. (2000). A phenology research on the main xylophyte in arid desert area: A example on cultivated plants of Minqin Desert Botanical Garden. *Xibei Zhiwu Xuebao,* **20**, 1102-1109.

Zaady, E., Karnieli, A., & Shachak, M. (2007). Applying a field spectroscopy technique for assessing successional trends of biological soil crusts in a semi-arid environment. *Journal of Arid Environments,* **70**, 463-477.

Zarco-Tejada, P.J., Pushnik, J.C., Dobrowski, S., & Ustin, S.L. (2003). Steady-state chlorophyll a fluorescence detection from canopy derivative reflectance and double-peak red-edge effects. *Remote Sensing of Environment,* **84**, 283-294.

Zhang, J. (2010). Multi-source remote sensing data fusion: status and trends. *International Journal of Image and Data Fusion,* **1**, 5-24.

Zhang, Y. (2004). Understanding image fusion. *Photogrammetric Engineering and Remote Sensing,* **70**, 657-661.

Zhao, K., Valle, D., Popescu, S., Zhang, X., & Mallick, B. (2013). Hyperspectral remote sensing of plant biochemistry using Bayesian model averaging with variable and band selection. *Remote Sensing of Environment,* **132**, 102-119.

Table 1: List of the past, present, and forthcoming high spatial resolution satellites along with their spectral characteristics. (List partially provided by Abraham Tal)

Satellite	**Country**	**Launch year**	**Bands in spectral regions**		
			Panchromatic	**VNIR**	**SWIR**
			Resolution (m)	**No. of bands/ resolution (m)**	**No. of bands/ resolution (m)**
Ikonos*	USA	1998	0.8	4X3.2	
QuickBird*	USA	2001	0.6	4X2.16	
Formasat 2	Taiwan	2004	2.0	X8	
WorldView 1	USA	2007	0.5		
GeoEye 1	USA	2008	0.4	4X1.65	
RapidEye 1-5	Germany	2008		5X6.5	
WorldView 2	USA	2009	0.3	8X1.2	
TH-01	China	2010	2.0	4X10	
Pléiades 1	France	2011	0.5	4X2.0	
KompSat 2	S. Korea	2012	1.0	4X4.0	
Pléiades 2	France	2012	0.5	4X2.0	
SPOT 6	France	2012	1.5	4X6.0	
Demios 2	Spain	2014	0.8	4X3.0	
SkySat	UK	2014	>1	3X2.0	
SPOT 7	France	2014	1.5	4X6.0	
WorldView 3	USA	2014	0.3	8X1.2	8X3.7
KompSat 3	S. Korea	2015	0.7	4X2.8	
WorldView 4	USA	2016	0.3	4X1.36	
VENμS	Israel/France	2017		12X5.3	

* system does not function anymore, archive data only.

Table 2: List of hyperspectral airborne scanners along with their spectral characteristics.

Sensor	Organization (country)	Spectral range (nm)	No. of bands	Spectral resolution (nm)
DAIS 7915	DLR (Germany)	400-12600	79	1,45
PROB-1	Earth Search Sciences Inc. (USA)	400-2500	128	12,16
HyMap	HyVista Corp. (Australia)	450-2500	132	15,20
CASI-1500	ITRES (Canada)	365-1050	288	3.5
SASI	ITRES (Canada)	950-2450	100	15
SFI	CCRS (Canada)	1208-2445	120	10.3
AVIRIS	NASA (USA)	400-2500	244	10
AISA DUAL	Specim (Finland)	400-2450	498	2.9,8.5
VNIR-640	HySpex (UK)	400-1000	128	5
Hyperspec	Headwall (USA)	400-2500	333	5,10
CAO VSWIR	Carnegie Airborne Observatory (USA)	380-2510	428	5
TRWIS III	TRW Space and Electronics Group (USA)	400-2450	384	5.25,6.25

Table 3: List of the in-orbit, under construction, and forthcoming hyperspectral satellites along with their spectral characteristics. (Data compiled by Eyal Ben Dor)

Sensor	Organization (country)	GSD (m)	Swath at nadir (km)	Spectral range (nm)	Number of bands	Spectral resolution (nm @FWHM)	Launch date	Status
Missions currently in orbit								
Hyperion	NASA (USA)	30	7.65	375-2576	242	10	2000	**Missions currently in orbit**
CHRIS	ESA (UK)	17/34	13 (nominal)	400-1050	18/63	5.6-32.9	2001	
HJ-1A	CAST (China)	100	≥50	450-950	110-128	5	2008	
HySI	ISRO (India)	506	129.5	450-950	64	~10	2008	
HICO	NASA/ONR (USA)	90	42	353-1081	128	5.7	2009	
Missions under construction								
GISAT	ISRO (India)	500	NA	NA	210	NA		**Missions under construction**
PRISMA	ASI (Italy)	30	30	400-2500	237	~12		
HISUI	METI (Japan)	30	15	400-2500	185	10 (VNIR) 12.5 (SWIR)		
EnMAP	DLR/GFZ (Germamy)	30	30	420-2450	218	5/10 (VNIR) 10 (SWIR)		
Missions in the planning stage								
FLORIS/FLEX	ESA	300	100-150	500-780	NA	0.3-3.0		**Missions in the planning stage**
HYPXIM-P	CNES (France)	8	16	400-2500	>200	≤10		
HyspIPI	NASA (USA)	60	145	380-2500	>200	10		
SHALOM	ISA/ASI (Israel/Italy)	10/5	10	400-2500	200	10		

Table 4: Main biological pigments and the central location of their absorption features.

	In vivo	***In situ***
Chlorophyll-a	430, 660	450, 670
Chlorophyll-b	450, 650	
Carotenoids	445	500
β-carotene	470	
Anthocyanins	530	550

Table 5: Major absorption features for cellulose, lignin, and protein (after Ben Dor et al. 1997).

Wavelength (nm)	Soil organic matter component
1203	Cellulose
1358	Cellulose, Lignin
1367	Cellulose, Lignin
1465	Cellulose, Lignin
1468	Cellulose, Lignin
1582-3	Cellulose
1726	Cellulose, Lignin
1761	Cellulose, Lignin
1769	Cellulose, Lignin
1929-32	Cellulose, Lignin
2068	Cellulose
2111	Cellulose
2142	Lignin
2169	Lignin
2193	Protein
2331	Cellulose, Lignin
2347	Cellulose, Lignin
2386	Protein

Table 6: Key ecological variables with respect to their analysis mean, main spectral bands, and type of remote sensing platform.

	Ecosystem variable / Ecological application	Analysis means	Main spectral bands	Remote sensing platform
Structural vegetation properties	Leaf area index (LAI),	Vgetation indices	VNIR	Broadband
	Fractional vegetation cover	Vgetation indices	VNIR	Broadband
	Above-ground biomass	Vgetation indices	VNIR	Broadband
	Fraction of absorbed photosynthetically active radiation (fAPAR)	Vgetation indices	VNIR	Broadband
	Net Primary Productivity (NPP)	Vgetation indices	VNIR	Broadband
	Foliar loss and damage	Vgetation indices	VNIR	Broadband
Fine spectral vegetation features	Chlorophyll content	Spectral indices	VIS, Red-edge	Narrowband
	Carotenoid pigment	Spectral indices	VIS, Red-edge	Narrowband
	Anthocyanin pigment	Spectral indices	VIS, Red-edge	Narrowband
Nutrients	Nitrogen	Spectral indices	VNIR (indirect); 1510 nm (direct)	Narrowband
	Potassium (K)	Multivariate analysis		Narrowband
	Phosphorus (P)	Multivariate analysis		Narrowband
Soil organic matter	Lignin	Multivariate analysis	SWIR	Narrowband
	Cellulose	Multivariate analysis	SWIR	Narrowband
	Protein	Multivariate analysis	SWIR	Narrowband
Vegetation water content	Canopy water content	Spectral indices	NIR, SWIR	Broadband
	Leaf water potential	Spectral indices	NIR, SWIR	Narrowband
	Stomatal conductance	Spectral indices	NIR, SWIR	Narrowband
	Non-photochemical quenching	Spectral indices	NIR, SWIR	Narrowband

Soil	Soil moisture	Spectral indices	NIR, SWIR	Broadband
	Brightness	Spectral indices	VIS	Broadband
	Ferric oxides	Spectral indices	VIS	Broadband
	Hematite minerals	Spectral indices	VIS	Broadband
	Clay minerals	Spectral indices	SWIR	Broadband
	Ferrous minerals	Spectral indices	SWIR	Broadband
	Soil oxidation	Spectral indices	VIS	Broadband
	Biocrusts	Spectral indices	VIS	Broadband
Albedo	Surface albedo	Spectral bands	VIS-NIR-SWIR	Broadband
Snow	Snow cover	Spectral indices	VIS, SWIR	Broadband
Fire scars	Fire scars area	Spectral indices	NIR, SWIR	Broadband

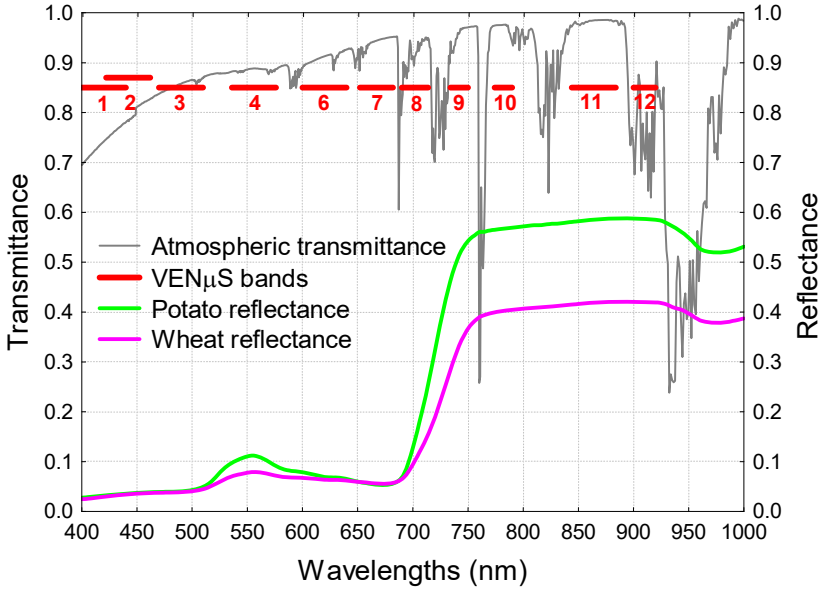

Figure 1: Band settings of VENμS with respect to the atmospheric transmittance and typical vegetation reflectance spectra.

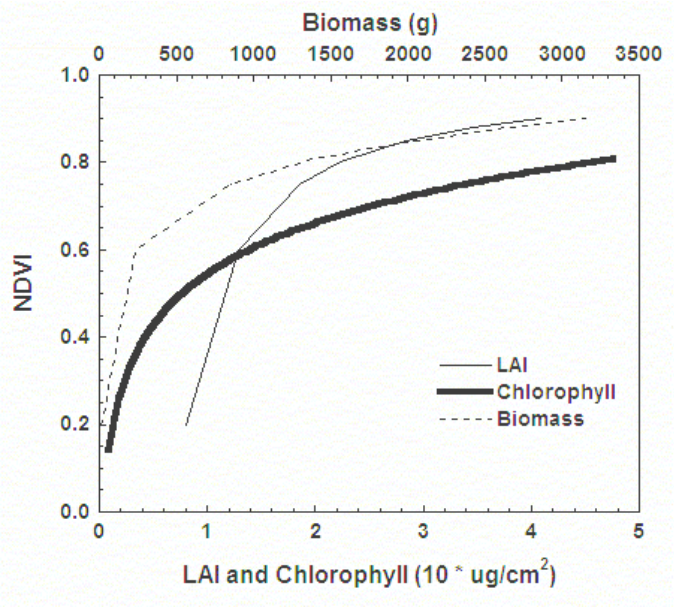

Figure 2: The Normalized Difference Vegetation Index (NDVI) as a function of Leaf Area Index (LAI), chlorophyll content, and biomass. Note the less sensitivity ('saturation') of the NDVI when high values of the independed variables are presented, indicating dense and multilayered canopies. (Data provided by Agustin Pimstein and Ittai Herrmann).

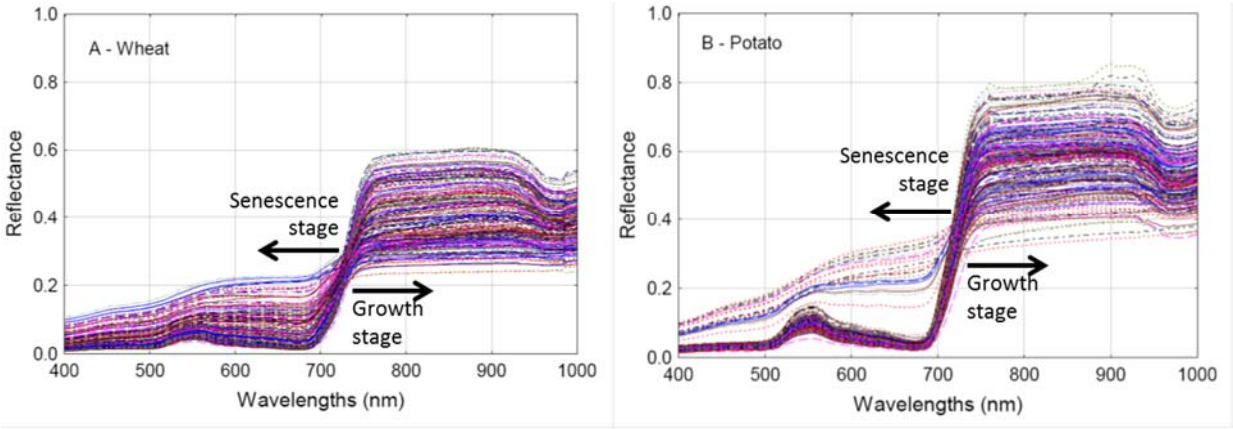

Figure 3: Temporal dynamics of the red-edge during the phenological cycles of wheat (A) and potato (B) crops. (Data provided by Agustin Pimstein and Ittai Herrmann)